NONACCELERATOR-BASED NEUTRINO OSCILLATION EXPERIMENTS

Kai Martens*
Institute for Cosmic Ray Research, University of Tokyo
Kamioka Observatory
Higashi-Mozumi, Kamioka-Cho, Yoshiki-Gun, 506-1205 Gifu-Ken, Japan

ABSTRACT

The experimental effort dedicated to understanding the nature of the Solar Neutrino Problem is presented and the atmospheric neutrino anomaly reviewed.

*Supported by the Japan Society for the Promotion of Science.

1 Introduction

In the quest for an answer to the fundamental question of whether or not neutrinos are massive particles, neutrino oscillation has taken center stage. Were neutrinos found to oscillate from one flavor to another, nonzero neutrino mass would be the direct consequence. While some claim that neutrino oscillation may thus become the first step beyond the minimal Standard Model of particle physics, others accept nonzero neutrino mass as an unsurprising fact in the context of a more modern view of what a standard model for particle physics is. Agreement however seems to exist that neutrino masses are fundamental parameters of extreme importance and that given the current experimental situation, finding evidence for neutrino flavor oscillation is our best chance to obtain direct evidence for a nonzero neutrino mass.

Three experimental observations are currently inspiring interpretations in terms of neutrino oscillation:

- the Solar Neutrino Problem
- the Atmospheric Neutrino Anomaly
- results from the Liquid Scintillator Neutrino Detector (LSND) experiment at the Los Alamos Meson/Proton Factory (LAMPF).

The solar neutrino problem is the longest-standing among these. Solar neutrinos and the solar neutrino problem as it presents itself today are introduced in a separate lecture by J. N. Bahcall,[1] which allows me to concentrate on the experimental techniques employed in solar neutrino observation and the impressive experimental effort currently aimed at understanding the true nature of the solar neutrino problem.

For atmospheric neutrinos, a different attitude has to be taken. No separate lecture covers the theoretical backdrop to the phenomenology of the field, and the present atmospheric neutrino anomaly must be introduced in its context of flux calculations for secondaries of particle interactions in the high atmosphere. Since this task in itself could easily fill a series of lectures, I will restrict myself to providing an outline of the problems involved; these affect the forms chosen to present and interpret the data. Atmospheric neutrinos are typically observed as by-products in proton decay experiments or WIMP (Weakly Interacting Massive Particle) searches. Unlike solar neutrinos, no dedicated experimental program

exists exclusively for atmospheric neutrinos. In the foreseeable future it is again mostly proton decay experiments that are expected to produce more detailed results on atmospheric neutrinos. The oscillation parameter range implicated in an oscillation analysis of the anomaly will ultimately be addressed by long baseline experiments.

The third item on our list of experimental results commonly interpreted in terms of neutrino oscillations—data from the LSND experiment—is accelerator-based and therefore discussed in the lectures of S. Wojcicki.[2]

None of the three experimentally observed anomalies is as yet accepted as a solid case for neutrino oscillation. In fact, to simultaneously interpret all three as manifestations of neutrino oscillation, more than three neutrino species would be required; a fact seen by many as indicative of a problem with at least one of the experimental results.

2 Solar Neutrinos

The solar neutrino problem has evolved over the last 30 years. The first solar neutrinos were detected by the Homestake chlorine experiment in 1970.[3] In 1987, Kamiokande became the second experiment to observe solar neutrinos and the first to unambiguously link its neutrino signal to the sun.[4] Their method of real-time directional solar neutrino observation allowed them to point back to the source moving across the sky. Since 1990, gallium experiments[5,6] have lowered the energy threshold of solar neutrino detection to reach into the energy spectrum of neutrinos produced in the first step of the sun's fundamental energy-generating process—the fusion of two protons into a deuterium nucleus.

The solar fuel cycle ultimately fuses protons into ^{4}He nuclei. This proceeds through a variety of reactions, some of them competing with each other. The ones involving the emission of neutrinos are listed in Table 1.

Depending on the reaction, the neutrino energy will either be a continuous spectrum, reaching up to a specific endpoint energy, or a line at a well-defined neutrino energy. Figure 1 gives an idea of the expected intensities for the associated fluxes, as calculated from the 1995 solar model of J. N. Bahcall and M. H. Pinsonneault (BP95).[7] The BP95 solar model is one of a now highly constrained class of solar models that accommodate the observational data available from helioseismology.[8] Until the advent of these data, particle physics conclusions

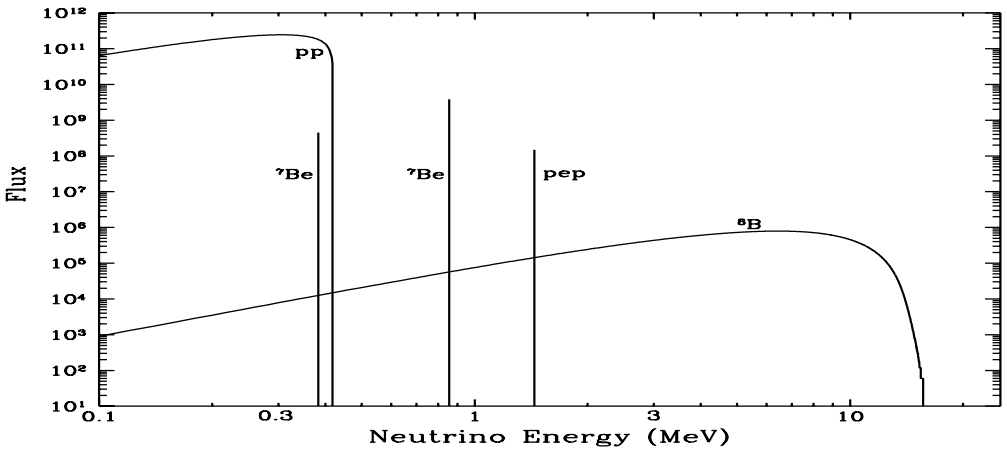

Fig. 1. Solar neutrino fluxes at Earth according to BP95 (taken from J. N. Bahcall's webpage: http://www.sns.ias.edu/∼jnb/SNviewgraphs/snviewgraphs.html). Neutrinos from the CNO cycle are not shown.

Reaction	Spectrum	Energy
He fusion chain		
$p + p \to {}^2H + e^+ + \nu_e$	endpoint:	420 keV
$p + e^- + p \to {}^2H + \nu_e$	line:	1.442 MeV
${}^7Be + e^- \to {}^7Li + \nu_e$	lines:	861 keV
		383 keV
${}^8B \to {}^8Be + e^+ + \nu_e$	endpoint:	14.1 MeV
${}^3He + p \to {}^4He + e^+ + \nu_e$	endpoint:	18.77 MeV
CNO cycle		
${}^{13}N \to {}^{13}C + e^+ + \nu_e$	endpoint:	1.199 MeV
${}^{15}O \to {}^{15}N + e^+ + \nu_e$	endpoint:	1.732 MeV
${}^{17}F \to {}^{17}O + e^+ + \nu_e$	endpoint:	1.740 MeV

Table 1. Neutrino-emitting reactions in the sun.

from the solar neutrino problem were tempered by a healthy suspicion towards the reliability of solar models, and modifications to solar modeling were contrived to alleviate discrepancies. Yet so far only models that are indistinguishable from the point of view of their predictions for solar neutrino experiments can reproduce the helioseismological data.

All neutrinos generated by the reactions in the solar core are ν_e. Were ν_μ or ν_τ found to be coming from the sun, then ν_e must have oscillated into these species. Since a direct observation of the heavier leptons created in charged current reactions is experimentally difficult at low energies, comparing the charged current (CC) to neutral current (NC) reaction ratio in solar neutrino interactions is the only viable way to directly check for oscillations into the other known neutrino species.*

The lectures on solar neutrinos are organized by experimental techniques. A radiochemical experiment was the first to observe solar neutrinos, and the first lecture will cover the underlying experimental technique and its implementations. A water Cherenkov detector provided the first directional solar neutrino signal, thus unambiguously identifying its source. This currently very active field will be surveyed in the second lecture. In the final lecture, I will summarize the present ideas about real-time experiments to come.

2.1 Radiochemical Experiments

The radiochemical method for neutrino detection was first proposed by Bruno Pontecorvo in 1946 as a means for an experimental verification of the neutrino's existence.[9] It exploits the inverse β-decay reaction, which changes the atomic number, and therefore, the chemical properties of the target atoms X:

$$\nu_e + {}^{\mathrm{A}}_{\mathrm{Z}} X \rightarrow {}^{\mathrm{A}}_{\mathrm{Z+1}} Y + e^-.$$

The idea is to isolate the few atoms of the new element Y produced by neutrino interaction from the bulk mass of target atoms by means of their distinct chemical properties. With the target atoms properly chosen, the produced β-unstable atoms Y can then be counted by their characteristic β-decay.

Suitable materials should be inexpensive, given the large target masses the cross sections require. The β-unstable species produced by inverse β-decay should

*The existence of ν_τ still awaits direct experimental verification.

have a lifetime long enough to allow for extraction, and short enough to allow for subsequent counting of its decay. The extraction process itself should be simple and quantitative.

Consider a constant flux of neutrinos Φ incident on a material containing N_X target atoms with a cross section σ for inverse β-decay. If there is a constant background rate $\mathrm{R_{BG}}$ at which the product nuclei are produced in the material by means other than inverse β-decay on the target X [e.g., (p, n) exchange reactions on X], the number of product atoms N_Y accumulated after a given time t will be

$$N_Y = (\sigma\Phi + \mathrm{R_{BG}})N_X\tau_Y(1 - \mathrm{e}^{-\frac{t}{\tau_Y}}),$$

where τ_Y is the lifetime of the produced isotope Y. If ϵ_E is the extraction efficiency, and ϵ_C the efficiency for identifying the product decays in the subsequent counting procedure, the number N_{obs} of presumably observed neutrino interactions is given by

$$N_{obs} = N_Y \times \epsilon_E \times \epsilon_C,$$

and the measured product of neutrino flux and cross section $\Phi\sigma_{obs}$ after background subtraction becomes

$$\Phi\sigma_{obs} = \frac{N_{obs}}{N_X\tau_Y(1-e^{-\frac{t}{\tau_Y}})\epsilon_E\epsilon_C} - \mathrm{R_{BG}}.$$

To extract the neutrino flux, the cross section must evidently be known. The threshold for inverse β-decay is related to the endpoint energy of the corresponding β-decay process. If the β-decay proceeds through electron capture in a ground-state to ground-state transition between the nuclei involved, the cross section for the inverse process can be extracted from the lifetime. This requires calculation of electron and nucleon wave function overlap and of the relative rates of captures from the K and L atomic shells to be known. The treatment of transitions involving excited states is much more complicated and the degree of confidence in the calculation depends heavily on the isotopes involved.[10]

Careful consideration must be given to the evaluation of extraction and counting efficiency, as well as the rate of producing the isotope of interest through processes other than inverse β-decay. Since the Sun will hopefully not shut down soon, this background rate cannot be measured directly.

The above formula can be used to derive the maximum number of inverse β-decay products a particular experiment can accumulate in the limit of infinite

exposure. After a sufficiently long time, production and decay of the β-unstable isotope will equilibrate, and a single extraction can yield at most

$$N_Y(t \to \infty) = (\sigma\Phi + \mathrm{R_{BG}})\mathrm{N_X}\tau_\mathrm{Y}$$

atoms for the subsequent counting process. This value is crucial in the design of a radiochemical neutrino experiment. In real life, exposure will be limited to strike a balance between the expected signal and the integration time of the flux measurement. Also, some of the signal will decay before reaching the counting facility. Table 2 lists inverse β-decay candidates and some of their relevant properties.

Target	Natural Abundance	Product	Half-Life	Threshold
^{7}Li	92.5%	^{7}Be	53 d	862 keV
^{37}Cl	24.2%	^{37}Ar	35 d	814 keV
^{51}V	99.7%	^{51}Cr	28 d	751 keV
^{55}Mn	100%	^{55}Fe	3 y	231 keV
^{71}Ga	39.9%	^{71}Ge	11 d	236 keV
^{81}Br	49.3%	^{81}Kr	2.3×10^5 y	459 keV
^{87}Rb	27.8%	^{87}Sr	3 h	115 keV
^{115}In	95.7%	^{115}Sn	3×10^{-6} s	120 keV
^{127}I	100%	^{127}Xe	36 d	789 keV
^{205}Tl	70.5%	^{205}Pb	1.5×10^7 y	62 keV

Table 2. Inverse β-decay candidates for solar neutrino experiments.

A special unit was invented to discuss (radiochemical) solar neutrino experiments: The SNU (Solar Neutrino Unit). It is simply defined as 10^{-36} interactions per target atom per second. The factor 10^{-36} is motivated by the magnitude of the fluxes ($\sim 10^{10}\,\mathrm{cm^{-2}s^{-1}}$) and cross sections ($\sim 10^{-46}\,\mathrm{cm^2}$) involved.

The requirement of simple extraction led Pontecorvo to suggest stable products of β-decay of noble gases as targets. Since noble gases are chemically inert, quantitative extraction can easily be achieved by physical methods. Pontecorvo specifically pointed out the reaction $\nu_e + {}^{37}\mathrm{Cl} \to {}^{37}\mathrm{Ar} + \mathrm{e}^-$, which 20 years later was used in the first experiment to observe solar neutrinos: the Homestake solar neutrino experiment.

2.1.1 The Chlorine Experiment

Installation of the first solar neutrino experiment started in the Homestake Gold Mine at Lead, South Dakota, USA, in 1965. The reaction used to detect solar neutrinos is inverse β-decay on a ^{37}Cl target. It is sensitive only to electron-type neutrinos with energies above 814 keV. Neglecting the CNO cycle and hep neutrinos, these are the high energy neutrinos from the ^{8}B spectrum as well as the higher energy ^{7}Be line and the pep line.

The experiment is located 1480 m underground, shielded by an overburden of 4200 MWE.[†] Construction was completed by 1967. A cylindrical 400,000-liter tank 6.1 m in diameter and 14.6 m long contains 615 tons of perchloroethylene (C_2Cl_4), thus 2.2×10^{30} atoms of the target isotope ^{37}Cl (Fig. 2). The atmosphere above the target liquid is helium, and the whole system, including all piping, is kept at an overpressure of 1/2 atm. This prevents the admission of argon and especially the radioactive isotopes of radon and krypton from the mine air. The target liquid is typically exposed to solar neutrinos for two months before extraction of the produced ^{37}Ar.

To extract argon, the target liquid is purged with helium. During extraction, pumps circulating the liquid in a closed loop at high pressure draw in helium from the top of the tank through Bernoulli nozzles and mix it with the liquid. Two of these nozzles draw helium together with some perchloroethylene vapor and the argon from the top of the tank through the argon extraction system. A condenser at $-40\,^{\circ}$C and a molecular sieve remove the perchloroethylene vapor. The molecular sieve is the only part in the system that is changed regularly. Argon is recovered in a subsequent charcoal trap at liquid nitrogen temperature.

To monitor the extraction efficiency, known amounts of stable argon isotopes are added to the target fluid at the beginning of each solar run. To tag the argon added in a specific run, it is isotopically enriched by either ^{36}Ar or ^{38}Ar. Extraction, which has a time constant of 400 min, proceeds over a 20 h period and argon recovery efficiency is found stable at 90–95% over the three decades of lifetime the experiment accumulated by now. Uncertainty in the extraction efficiency contributes 0.3% to the systematic error of the overall result quoted below. Isotopic analysis of the recovered argon is performed after counting of the ^{37}Ar decays is completed.

[†]MWE = Meters Water Equivalent.

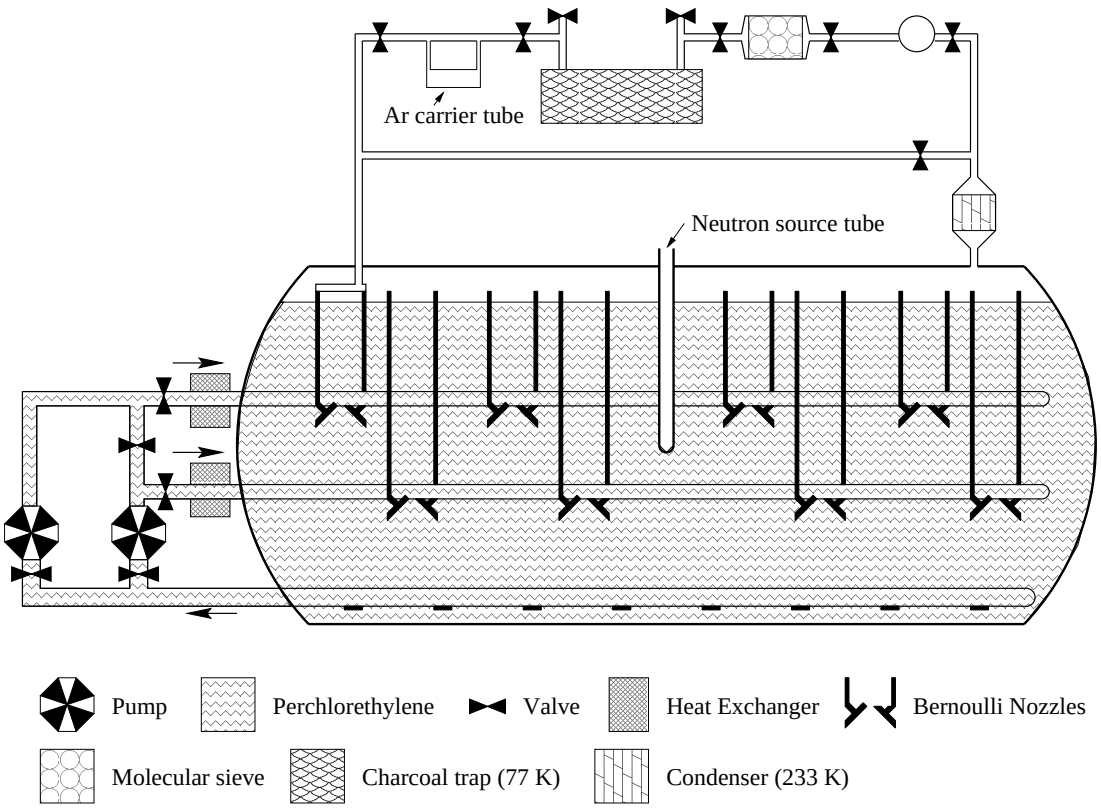

Fig. 2. Schematic view of the Homestake Chlorine Detector. The figure is an adaption from Fig. 1, page 1206, in Ref. 14. The number of Bernoulli nozzles is 40 in the real detector. Note that two of these are used to circulate the helium through the extraction system.

The most important background process to ^{37}Ar production by inverse β-decay is the reaction in which ^{37}Cl captures a proton and releases a neutron to become ^{37}Ar. Since the results of the two processes are indistinguishable, measurements of reactions releasing protons in the target liquid had to be carried out to get an estimate of the expected background rates. Protons may arise as spallation products of cosmic ray muon interactions, fast neutrons being captured on ^{35}Cl (natural isotopic abundance 76%) to form ^{35}S, and α-particles being captured on ^{35}Cl to produce ^{38}Ar.

Measurements of ^{37}Ar production at different depths in the mine led to an estimate for the background production rate from cosmic ray muons of 0.047 ± 0.013 ^{37}Ar/d. Fast neutrons emerging from the surrounding rock can be shielded by water. In 1971, the cavity containing the experiment was flooded for this purpose. In 1986, the water shield was replaced by a 30 cm liquid scintillator shield surrounding the tank. Neutrons were measured using neutron capture on ^{40}Ca in a radiochemical neutron detector, resulting in an estimated contribution of 0.030 ± 0.025 ^{37}Ar/d. In addition, α-capture reactions in the tank may release fast neutrons into the target liquid. Precautions against this possibility had already been taken in the construction of the experiment. The α-rate of the steel used to build the tank as well as the perchloroethylene used to fill it, was verified to conform with limits obtained from experiments on the ^{37}Ar yield in perchloroethylene with ^{222}Rn as an α-emitter. α-rates on site were measured by direct counting, yielding an upper limit of 0.017 ^{37}Ar/d from α-induced proton release. No shielding can eliminate the background from atmospheric neutrino induced inverse β-decay on the ^{37}Cl. The estimated upper limit is 0.0012 ^{37}Ar/d. Direct production of ^{37}Ar by α-particle and γ-ray absorption on ^{34}S and ^{38}S contaminations respectively are negligible.

The extracted argon is subsequently purified by gas chromatography and transfered into a small proportional counter for low background counting of ^{37}Ar decays. The volume of these cylindrical counters is 0.5 cm^3, their radius 4 mm. Seven percent methane is added as a quencher. Although the argon half-life is 35 d, counting continues for 200–400 d to be sure the backgrounds to the counting procedure are measured precisely. During that period the counters remain in an active shield of NaI crystals to veto external contamination. In addition, the whole counting system is surrounded by a passive low radioactivity shield. Since 1977, counting has been performed in the mine to minimize interference from cosmic rays.

The decay proceeds via electron capture. Capture from the K-shell (90%) in ^{37}Ar results in emission of 3–4 Auger electrons (90%) with a total energy of 2.8 keV. The associated signal in the proportional counter is distinguishable from accidental single charged tracks by its fast risetime and its characteristic energy deposition. With typically only eight decays to be counted from a single extraction, background is the limiting factor when it comes to evaluating the data. For such an analysis a cut on risetime is made to retain only the fastest 10% of all events, and pulseheight is constrained to one FWHM (acceptance 76%) at the ^{37}Ar peak. Adding the data from many extractions allows statistically more significant measurements over longer observation periods. Here, systematic uncertainties incurred from the risetime and pulseheight cuts become important, and the cuts are relaxed accordingly. Uncertainties in the efficiency of the counting procedure contribute 1.5% to the systematic error of the experiment. Recalibration of the pulseheight scale is done at two-month intervals with a ^{55}Fe source during ^{37}Ar counting. A maximum-likelihood method is applied in order to extract the number of observed decays from the time sequence of counter events passing the risetime and pulse height cuts.[11] The time sequence is decomposed into a decay curve with the fixed half-life of 35 d and a constant background rate.

When the experiment was designed, best estimates for the product of cross section and solar neutrino flux for a chlorine experiment were as high as 40 SNU, yielding $N_{Ar}(t \to \infty) \simeq 450$ for the 2.2×10^{30} target atoms. By the time the experiment was built, various adjustments made on the cross sections used in solar models had brought this estimate into the range of present day values ($9.5^{+1.2}_{-1.4}$ SNU for BP95), corresponding to $N_{Ar}(t \to \infty) \simeq 110$. In 1968, when the first extractions were evaluated,[13] electronics for a risetime analysis of pulse shapes were not yet available. Thus, at the time only a discouraging upper limit of three SNU for the solar neutrino flux could be obtained. Only after this technique became available in late 1970 could a finite solar neutrino flux be measured for the first time. With one interruption (a liquid circulation pump failure brought the experiment down from May 1985 through October 1986), it has since accumulated data over 25 years—more than two solar activity cycles—for ^{7}Be and ^{8}B neutrinos from the sun.

The result obtained from a fit to the combined data of 108 extractions since 1970 was presented at the Neutrino '96 conference in Helsinki: $2.54 \pm 0.14(stat.) \pm 0.14(syst.)$ SNU (Ref. 14). For a discussion of various analyses of the ^{37}Cl database

in terms of time variations in the neutrino flux, see Ref. 15. Knowledge of the inverse β-decay cross section remains the limiting factor for the chlorine solar neutrino experiment.[12]

Plans for a Superchlorine detector with 3000 t of perchloroethylene at the Baksan Neutrino Observatory in the Caucasus mountains in Russia[16] unfortunately never came to pass.

2.1.2 The Gallium Experiments

The inverse β-decay of ^{71}Ga to ^{71}Ge has a threshold of 233 keV; this low threshold makes gallium experiments the only ones currently able to measure p-p neutrinos from the sun.[17] The natural isotopic abundance of ^{71}Ga is 39.9%. Since germanium is not a noble gas, extraction is more intricate than in the chlorine experiment. Two different methods of extracting germanium from vast amounts of gallium were developed independently. Both are implemented in either of the two gallium experiments: SAGE[5] [Russian (originally: Soviet) American Gallium Experiment] started solar neutrino observations in January 1990, GALLEX[6] (GALLium EXperiment) in May 1991.

SAGE is located in the Baksan Neutrino Observatory in the Northern Caucasus Mountains in Russia. Eight tanks (see Fig. 3) hold 55 t of metallic germanium as target, shielded from cosmic rays by an overburden of 4700 MWE. Approximately 700 μg of natural germanium carrier are evenly distributed among the eight tanks at the beginning of a typical one-month exposure. Chemical extraction proceeds by mixing the liquid gallium with a weak HCl solution in the presence of H_2O_2, thereby concentrating the germanium in the aqueous phase. The eight tanks are processed in parallel, and the combined extracted solutions are reduced in volume by vacuum evaporation. The addition of HCl produces $GeCl_4$, which is then purged into 1.2 liters of water.

GALLEX is located in the Gran Sasso Laboratory in Italy, shielded by an overburden of 3400 MWE. It uses 30.3 t of gallium in the form of a $GaCl_3$ solution (101 t) kept in a single tank (Fig. 4). The 1 mg germanium carrier admixed in the GALLEX experiment is cycled through isotopically distinct samples of ^{72}Ge, ^{74}Ge, and ^{76}Ge to allow the amount of germanium carried over from one run to the next to be measured. Extraction begins by purging the $GaCl_3$ solution with

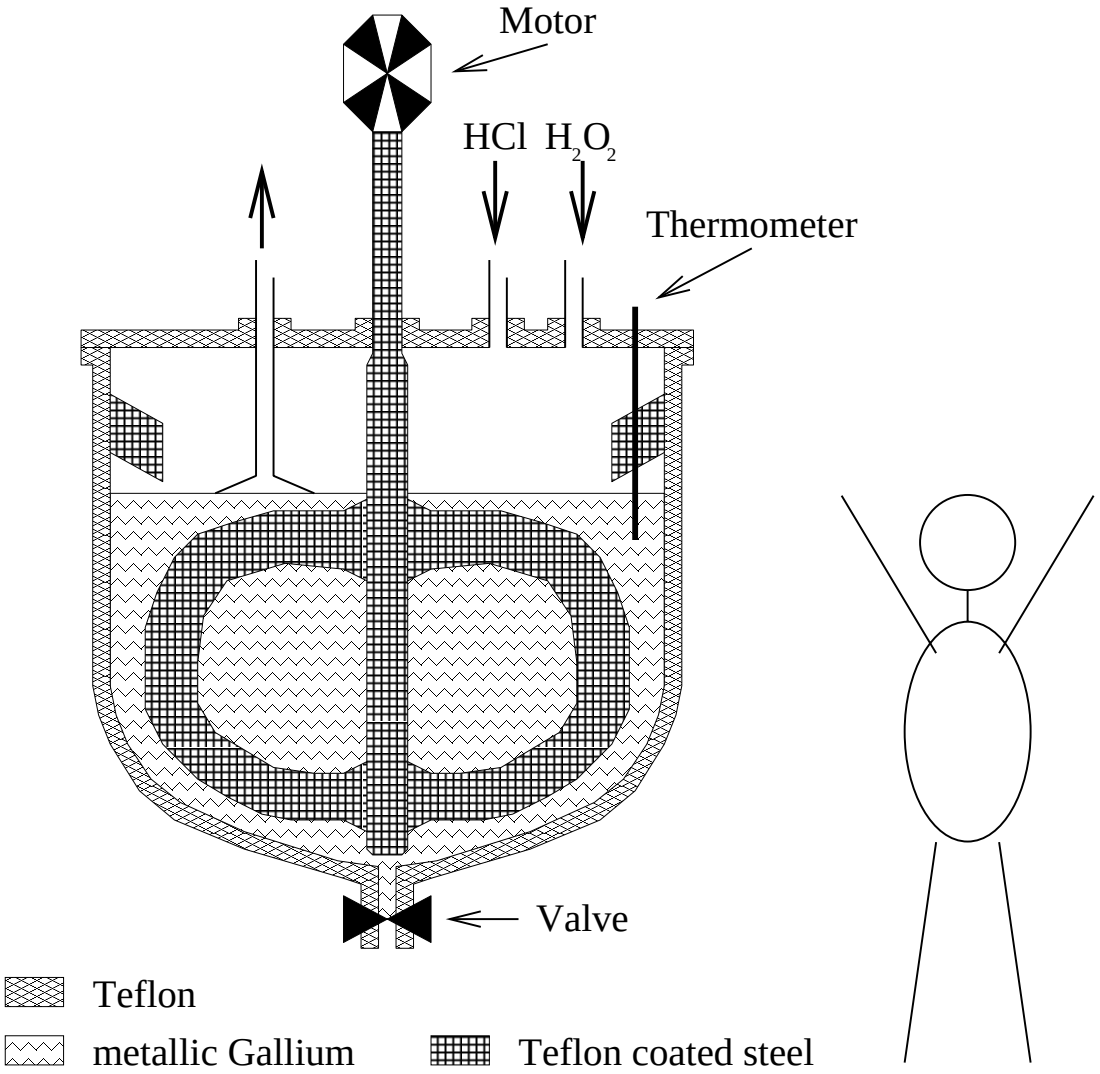

Fig. 3. One of the eight tanks holding metallic gallium in the SAGE experiment. The figure is inspired by transparencies made available by V. N. Gavrin, INR.

nitrogen. From the nitrogen, $GeCl_4$ is absorbed into water. After the addition of HCl, another purge with nitrogen extracts the $GeCl_4$ into one liter of water.

After the $GeCl_4$ solution is reduced in volume to about one liter, the extraction procedures of SAGE and GALLEX become identical. Extraction alternates several times between water and CCl_4, which finally is partially evaporated to reduce the total volume to about 0.1 liter. From this solution GeH_4 is synthesized and subsequently purified by gas chromatography. Xenon is added to obtain a counting gas mixture of Xe and GeH_4 (80%/20% in SAGE, 70%/30% in GALLEX) which is transferred into proportional counters for the measurement of ^{71}Ge decays. The extraction efficiencies quoted for the two experiments are $(80 \pm 6)\%$ for SAGE and between 95% and 98% for GALLEX. An extraction takes 30 min in SAGE and 20 h in GALLEX, while typical runs last for 28 d and 21 d, respectively. After extraction is completed, another 14 h will typically elapse in the GALLEX experiment before counting can begin.

The electron capture decay of ^{71}Ge proceeds via L-capture 10% of the time, releasing a 1.2 keV Auger electron. K-capture occurs 88% of the time; 42% of the K-captures result in the emission of a 10.4 keV electron and 41% produce a 9.2 keV γ-ray plus a 1.2 keV electron. Each experiment developed their own small, low-background counters (total volume 0.75 cm^3 for SAGE and 1 cm^3 for GALLEX). Xenon, with its short radiation length, allows conversion of the emitted γ-rays (mostly) inside the proportional counter's fiducial volume. During the counting process the counters are kept in an active shield of NaI crystals to veto external activity. GALLEX has counting sites with passive shielding in addition to those shielded by NaI. All counting proceeds on-site underground to minimize the background rate from cosmic rays.

The counters are calibrated at regular intervals during the measurement. SAGE uses an ^{55}Fe source at one-month intervals, while GALLEX exploits fluorescent γ-rays from the xenon in the counting gas at six-week intervals. The xenon-based counter calibration allows one to use three lines at 1.03, 5.09, and 9.75 keV. Counting continues for at least six months in GALLEX and for between two and six months in SAGE. The average number of observed decays in a single extraction is on the order of eight for SAGE and five for GALLEX.

The background production of ^{71}Ge during exposure again is linked to proton capture on the target nuclei, followed by neutron emission (threshold 1.02 MeV). Metallic gallium has an advantage over $GaCl_3$ in water here, as no free protons

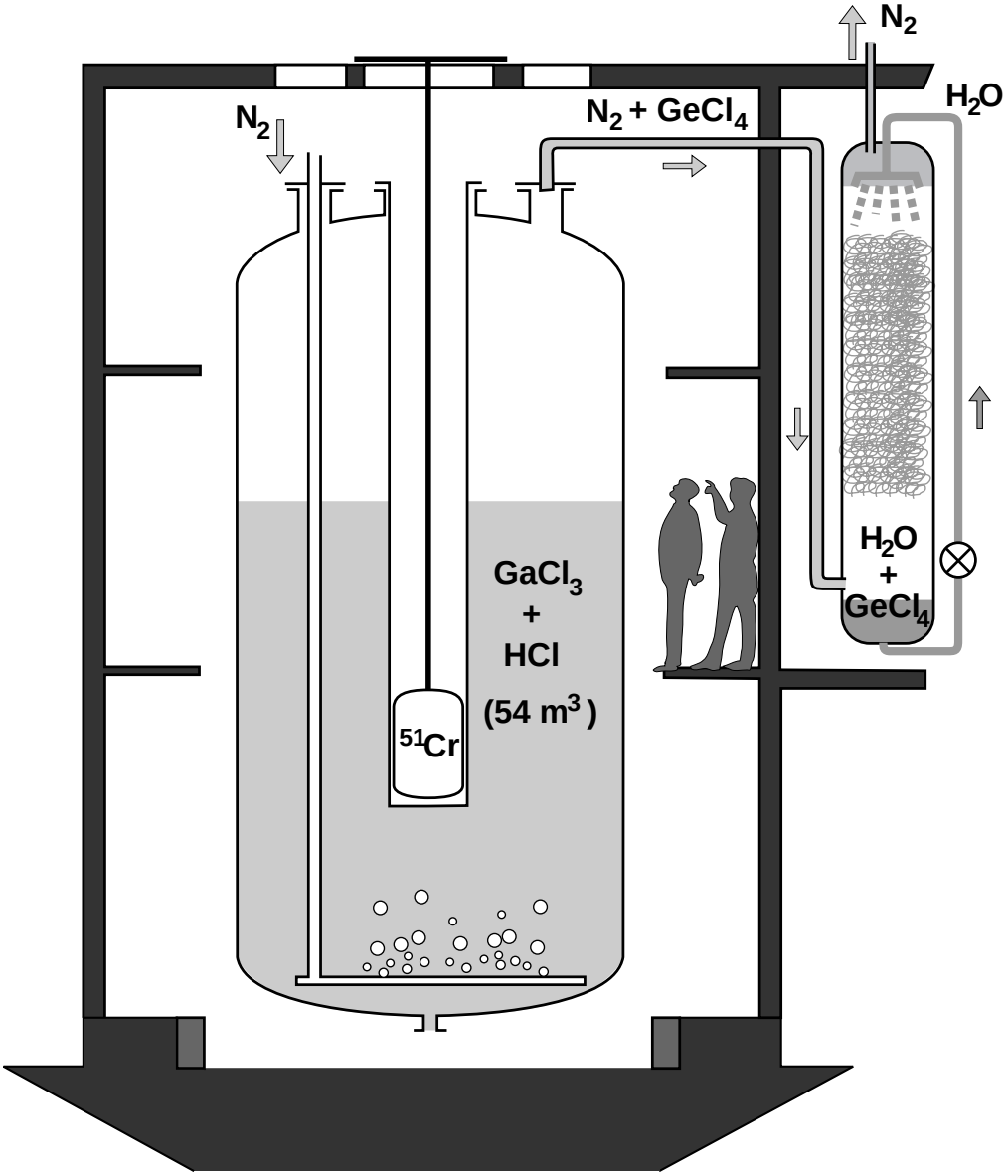

Fig. 4. The GALLEX tank with the source for ^{51}Cr calibration in place.

are available in the form of hydrogen nuclei. The two experiments express their respective background estimates differently. While SAGE gives an upper limit of ^{71}Ge nuclei produced per day from a specific source of background, GALLEX quotes the number of SNU it contributes to the measured signal. From the muon fluxes measured on-site they conclude $0.007\,\mathrm{d}^{-1}$ and (2.8 ± 0.6) SNU, respectively. GALLEX determined the ^{71}Ge yield in the $GaCl_3$ solution from muon irradiation in a dedicated experiment with a CERN muon beam. The fast neutron fluxes measured on-site correspond to $0.001\,\mathrm{d}^{-1}$ and (1.5 ± 0.1) SNU, and α-emitters in the decay chains of Uranium, Thorium, and ^{226}Ra contribute less than $0.015\,\mathrm{d}^{-1}$ and 0.2 SNU, respectively. Background to the counting procedure is linked to the decay chains of U, Th, and Rn, and cuts to eliminate the associated counts are based on the fact that α-decay events from these decay chains lead to counter overflow. Both experiments had to remove cosmogenic ^{68}Ge (half-life 271 d) that had been produced in the target materials before they reached their shielded underground sites.

The analysis techniques are those developed for the chlorine experiment: pulse-height and risetime analysis for event selection, followed by a maximum-likelihood fit to the time sequence. SAGE applies an asymmetrical time cut 20 min before and 180 min after events that lead to overflows, in order to reduce events associated with radon. GALLEX excludes events from 15 min before to 180 min after unvetoed overflows, and up to 180 min before event pairs consistent with a delayed coincidence between the ^{214}Bi β- and ^{214}Po α-decays. The efficiency of the counting process and analysis cuts is quoted to be 37% for the K-peak and 34% for the L-peak in SAGE and 35%(K)/31%(L) for GALLEX.

The solar neutrino fluxes measured by SAGE and GALLEX are 74^{+11+5}_{-10-7} SNU and $77 \pm 6 \pm 5$ SNU, respectively. SAGE data spans the period from January 1990 to November 1996, while GALLEX covers the interval from May 1991 to October 1995.

Tests with ^{51}Cr sources were performed by both experiments to verify efficiencies and cross sections.[18] The sources were prepared in nuclear reactors by neutron irradiation of chromium isotopically enriched in ^{50}Cr.[19] With a half-life of 27.7 d, ^{51}Cr decays by electron capture to ^{51}V, emitting monoenergetic neutrinos of 746 keV (81%), 751 keV (9%), 426 keV (9%), and 431 keV (1%). SAGE, with its modular structure of eight tanks of metallic gallium, irradiated two tanks with a source of (19.1 ± 0.2) Bq. In GALLEX the entire liquid target is held in

a single tank, which was designed to allow introduction of a source through a reentrant tube into the center of the tank. GALLEX performed two measurements with (63.4 ± 0.5) and (68.9 ± 0.6) Bq sources, using the same source after re-irradiating it.

The source strengths were each determined independently in different ways: From MC simulations of the reactor irradiation process, counting of the 320 keV γ-rays emitted in the de-excitation of ^{51}V produced in the decay of ^{51}Cr, and calorimetry. In summary, the source strengths measured by the gallium experiments found agreement at the 10% level with the cross sections and extraction and counting efficiencies used in their solar neutrino flux measurements. SAGE measured (95±11)% of the expected rate and GALLEX (99±11)% and (83±10)% for its two source experiments [combined: (91±8)%].

"Hot chemistry," i.e., the differences in chemical (and/or physical) behavior between atoms created by inverse β-reaction and atoms calmly residing in a solution, is an issue raised repeatedly throughout the history of radiochemical solar neutrino experiments. The fears were that such reactions could result in different extraction efficiency for the administered stable carrier germanium and the germanium produced in the inverse β-reaction. Such effects are ruled out by the ^{51}Cr source experiments to the level discussed above; yet even with the strongest neutrino sources ever produced, statistics limit the precision of these tests. Such statistical limitations can be overcome in arsenic spiking experiments. At the end of the GALLEX experiment, large quantities of ^{71}Ge were produced *in situ* from β-unstable ^{71}As. The decay ^{71}As to ^{71}Ge has a half-life of 2.7 d. A variety of experiments were carried out to test different aspects of the exposure and extraction procedures. Recovery from the tank was found to be quantitative in all cases, excluding any withholding mechanism at the 1% level.

The GALLEX experiment will find a continuation with the intention of enlarging the gallium target mass to decrease statistical uncertainty, and improving the counting procedure to reduce systematic errors. Under the new name of GNO (Gallium Neutrino Observatory) a long-term observation of the solar neutrino flux with a gallium detector is planned at the Gran Sasso underground laboratory. In the first stage, the experiment will continue where GALLEX ended, with the 30 t already on site. In 1999, one (now unused) of the two cylindrical tanks available at the laboratory will be filled in order to double the amount of gallium available for solar neutrino interactions. In a final expansion, 40 t of additional gallium would

make the final target mass 100 t. Whether this last addition of gallium again will be kept in a $GaCl_3$ solution or in metallic form will have to be decided. This final stage of the experiment is planned for after the year 2000.

If everything proceeds according to plan and nothing changes in the analysis chain, systematic errors arising in the counting procedure will soon dominate the flux measurement. Various improvements are currently under study, including the use of cryogenic detectors, which offer excellent energy resolution.

2.1.3 The Iodine Experiment

A new radiochemical experiment is currently being built in the Homestake Gold Mine at Lead, South Dakota, USA, at the same depth as the chlorine experiment. This experiment will use inverse β-decay on ^{127}I yielding ^{127}Xe. With a threshold of 789 keV, it will measure a mixture of ^{8}B, ^{7}Be, and pep neutrinos.

The natural isotopic abundance of ^{127}I is 100%. As with chlorine, the product is a noble gas, allowing the same extraction procedure based on physical principles and chemical inertness. A modular design allows continuous expansion from an initial target mass of 100 t (ten modules) to the final mass of 1000 t (5×10^{30} ^{127}I) (Ref. 14). The helium purge of the target solution is designed to have a time constant of only 11 min for this experiment, compared to 400 min for the chlorine experiment. A 99% efficient extraction can thus be completed in less than one hour, which will allow computer-controlled extraction to alternating charcoal traps every 12 hours, dividing the data into day and night samples. This is a unique feature in a radiochemical solar neutrino experiment. The time constant and uniformity of the ^{127}Xe extraction were verified in a prototype system.

The modules are cylindrical tanks of 1.2 m diameter and 11 m length, and each will be purged in parallel into a common xenon recovery system through its own liquid circulation system. Processing of the extracted gas will use the well-established procedures of the chlorine detector with two important exceptions: Two charcoal traps operated in parallel will separate the day and night samples, and the NaI counters surrounding the proportional counters during the counting process must be used in a different way. Since the ground state to ground state transition between the nuclei is forbidden, the β-decay of ^{127}Xe proceeds via excited states of ^{127}I, which decay under emission of one or more γ-rays. Thus, the

NaI crystals will be used to look for a signal coincident with the one from the proportional counter.

The process that allows the use of this coincidence technique is related to a problem which previously prevented this experiment. With the β-decay of ^{127}Xe going to excited states of ^{127}I, no normalization for the scaling of analog transition strengths in related nuclei can be extracted from a knowledge of the ground state transition strength, and the cross section for inverse β-decay is not known.[20,21] New nuclear physics experiments are under way to determine the relevant parameters, and there is confidence that this problem will soon be solved.

Background considerations are very similar to those for the chlorine experiment. Yet iodine enjoys a slight advantage, since its higher nuclear Coulomb field better protects the nucleus from encroaching protons.

2.2 Water Cherenkov Detectors

Cherenkov radiation is emitted by charged particles moving through a medium at a speed exceeding the speed of light in that medium. Its most striking characteristic is its emission into a cone around the particle's direction with an opening angle related to the velocity of the particle. This so-called Cherenkov angle θ_{ch} is determined by the particle velocity (expressed as the fraction β of the speed of light in vacuum) and the refractive index n of the medium: $\cos\theta_{ch} = \beta^{-1}n^{-1}$. For particles approaching $\beta = 1$ the Cherenkov angle attains a maximum value solely determined by the refractive index. Another important quantity is the threshold above which a particle emits Cherenkov light in the medium, given by the requirement $\beta > 1/n$. Cherenkov thresholds in water ($n = 1.35$) are given in Table 3.

Particle	Threshold
electron	760 keV
muon	160 MeV
pion	210 MeV
kaon	740 MeV
proton	1.4 GeV

Table 3. Cherenkov thresholds in water.

A water Cherenkov detector is a volume of water serving as radiator and equipped with light detectors to register the Cherenkov radiation emitted in the volume. Spherical detectors have no directional bias and are thus best suited for solar and atmospheric neutrino research. Low-energy neutrino interactions in water will typically yield an outgoing charged lepton with energy and direction related to the corresponding quantities of the incoming neutrino. The energy and direction of the outgoing charged lepton can be inferred from the amount of Cherenkov light emitted and the pattern created by the intersection of the Cherenkov cone with the photosensitive detector elements. Thus, water detectors are real-time detectors for neutrino interactions, with direction and energy resolution capabilities depending on the specific reaction employed.

The reaction observed in light-water Cherenkov detectors at solar neutrino energies is elastic scattering (ES) off electrons in the water. The nice feature of this reaction is a strong angular correlation between the outgoing electron and the incoming neutrino, allowing the projection of solar neutrino events back to the sun. The angular resolution of 20°–30° depends on the energy and is limited by multiple scattering, barring kinematic reconstruction of the energy of the incoming neutrino. However, the strong forward scattering peak clearly separates the signal from the isotropic background (see Fig. 6 in the section on the Kamiokande experiment). Unfortunately, the energy correlation in this reaction is very weak—the outgoing electron can have any kinetic energy between zero and the incoming neutrino energy. The spectrum of measured recoil electron energies therefore is a steeply falling one, making the flux measurement very sensitive to the detector's energy calibration.

Knowledge of the angular resolution as a function of energy is required to fit the solar neutrino forward scattering peak. The signal in Cherenkov detectors of the light-water type is extracted from a fit to the angular distribution of event directions with respect to the momentary direction to the sun at the time of each event. The fit assumes a solar neutrino peak of resolution appropriate for the energy of the events over an estimated background shape typically close to isotropic. If the cosines of the angles between direction to the sun and event direction are used, isotropy of the background translates into a constant offset from which the peak of solar neutrinos sticks out in the forward direction.

Complete isotropy of the background can be achieved in spherical detectors. A breaking of the spherical symmetry by the detector geometry may result in a non-

flat background distribution, if it introduces direction biases in the background event samples, as is the case for events induced by γ-rays from the surrounding rock in cylindrical detectors. If such events cannot efficiently be subtracted in the analysis, the proper background shape has to be taken into account. The impact of such effects is most keenly felt in the analysis of subsamples where the solar direction is restricted with respect to a detector's symmetry elements, for instance, in the analysis of day/night effects in cylindrical detectors.

The charged and neutral current reactions observable on deuterons in heavy-water Cherenkov detectors will be discussed in the context of the Sudbury Neutrino Observatory (SNO) experiment.

2.2.1 Kamiokande

Historically, Kamiokande was the second experiment to observe solar neutrinos, and the first to clearly identify the sun as the source of a neutrino signal: The real-time directional measurement projects its signal back to the sun. The Kamiokande experiment has now stopped, as a more powerful successor took over in 1996.

Kamiokande was originally designed as a proton decay experiment. Its cylindrical inner volume of 14.4 m diameter and 13.1 m height contained 4.5 kt of water, surrounded by 948 20-inch photomultiplier tubes. Several upgrades divide the live-time of the detector into three major phases: KAM I, KAM II, and KAM III. KAM I ran without an anticounter from June 1983 until November 1985. For KAM II an anticounter of 0.7–1.5 m thickness was added surrounding the inner detector volume. In addition to vetoing incoming or outgoing charged particles, it provided a passive shield against γ-rays emerging from nuclear reactions in the surrounding rock. To observe solar neutrinos, the electronics were upgraded to record timing information for individual hits. The water purification system was improved to keep thorium, uranium, and radon out of the detector water. In June of 1988, the gain of the inner detector's PMTs was doubled to increase single photoelectron efficiency. The operating period for KAM II was November 1985 through April 1990. KAM III (Fig. 5) resumed in December 1990 with new electronics and replacements for PMTs that had failed. The PMTs were now equipped with reflectors to enhance light collection efficiency, raising the effective photocathode coverage on the surface of the inner detector from 20% to 25%. A set of coils were installed around the detector to generate a magnetic field com-

pensating the earth's. Field compensation ensures uniform detection efficiency over the large photocathode area of the 20-inch PMTs.

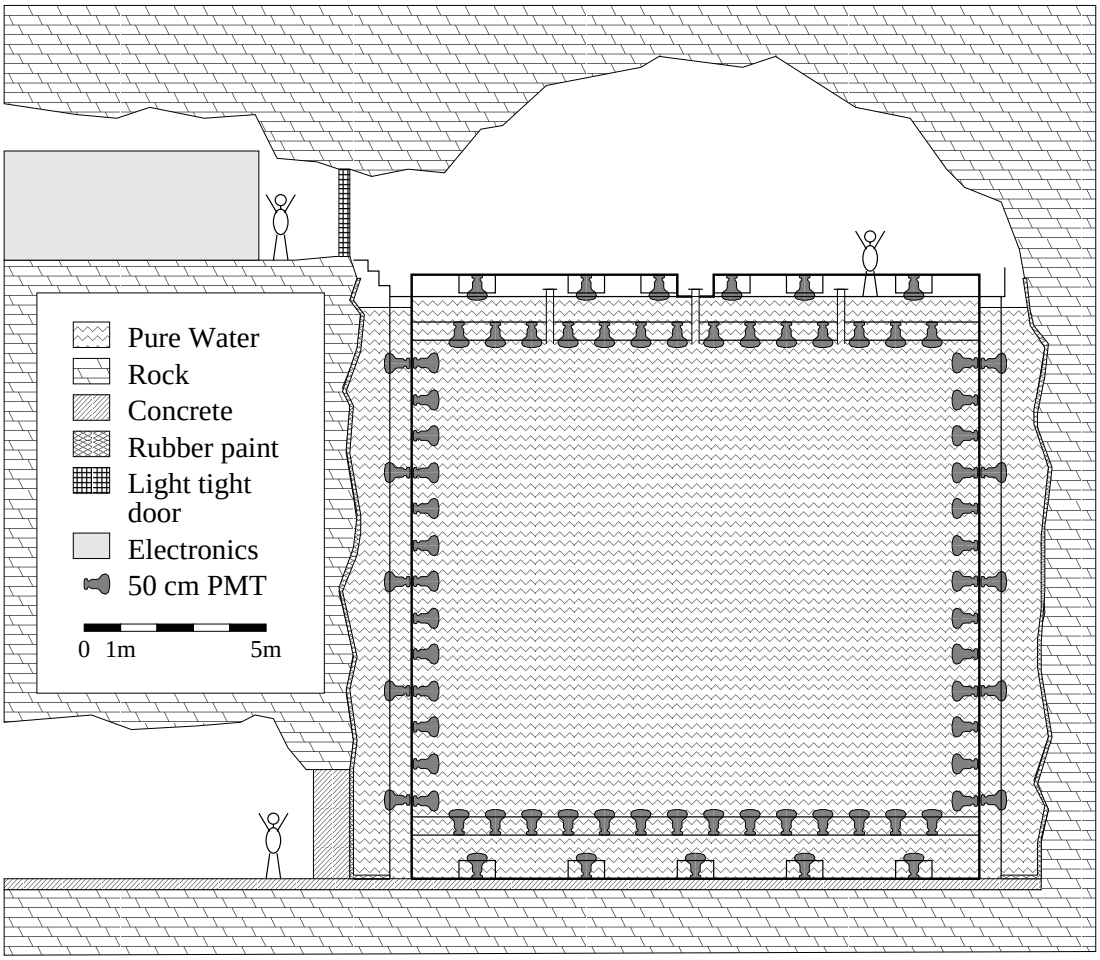

Fig. 5. The Kamiokande III detector. The reflectors mounted on the inner detector PMTs are not shown.

The trigger threshold for the KAM II detector was lowered in two steps from an initial 7.6 MeV down to 6 MeV, and the trigger threshold for KAM III reached 5 MeV. At that threshold 85,000 triggers were recorded per day, with three solar neutrino events per day expected from BP95.

Gamma rays with an average energy of $\sim$ 9 MeV from a nickel/californium source were used to calibrate the energy scale for solar neutrino events in the Kamiokande detector. In this source, neutrons from the fission of ^{252}Cf are thermalized in detector water that floods the space between the central fission source and a confining can made of nickel, in which the desired γ lines are produced by

neutron capture on ^{58}Ni. To subtract the background from the low-energy γ rays associated with the de-excitation of the fission fragments, background runs were taken with the nickel replaced by a polyethylene can. Comparison with Monte Carlo (MC) events simulating the nickel γ events fixed the energy scale for the solar neutrino events in Kamiokande. The photo-electron yield in KAM III was four hits/MeV.

The systematic error introduced to the total ^{8}B neutrino flux measurement through the remaining uncertainty in the energy scale was estimated to be 5.3%. With no directional calibration source of electrons available, the largest contribution to this measurement's systematic error, amounting to 7%, came from the uncertainty in the angular resolution of the detector. Apart from 4% from the fiducial volume cut, all further contributions are below 1%, adding quadratically to the total systematic error on the flux of 9.7% quoted for KAM III.

The background in the final Kamiokande solar neutrino sample consisted mainly of radon (30%), γ-rays from the surrounding rock (25%), and spallation ($< 25\%$). Radon contributes through the β-decay of ^{214}Bi in its decay chain, and was specifically targeted in the water purification system. The Kamioka site, unfortunately, is not deep enough to completely suppress cosmic ray muons and prevent them from producing radioactive spallation products when passing through the detector volume. To some extent, events produced by the decays of radioactive spallation products can be removed from the event sample by means of their correlation with the preceding muons.

Solar neutrino observation with KAM II consisted of a total live-time of 1043 days from January 1987 to April 1990 (Ref. 22). Of these, 449 days were analyzed above a threshold of 9.3 MeV, and the remaining 594 days above 7.5 MeV, yielding a flux extrapolated over the full ^{8}B neutrino spectrum of $2.77^{+0.31}_{-0.30}(stat.) \pm 0.39(syst.) \times 10^6\,\mathrm{cm}^{-2}\mathrm{s}^{-1}$. KAM III accumulated another 1036 days of solar neutrino data between December 28, 1990 and February 6, 1995. With an analysis threshold of 7.5 MeV for 200 days and 7 MeV for the remainder, the total flux measured in KAM III was $2.82^{+0.25}_{-0.24}(stat.) \pm 0.27(syst.) \times 10^6\,\mathrm{cm}^{-2}\mathrm{s}^{-1}$. The improvement in the systematic error between KAM II to KAM III was due to improved stability of the energy calibration. The final result for the combined data from KAM II and KAM III is $2.80 \pm 0.19 \pm 0.39 \times 10^6\,\mathrm{cm}^{-2}\mathrm{s}^{-1}$, the error thus clearly being dominated by systematics. The final solar neutrino peak for the Kamiokande

experiment contains 600 solar neutrino events from 2079 days of observation with a fiducial volume of 680 t.

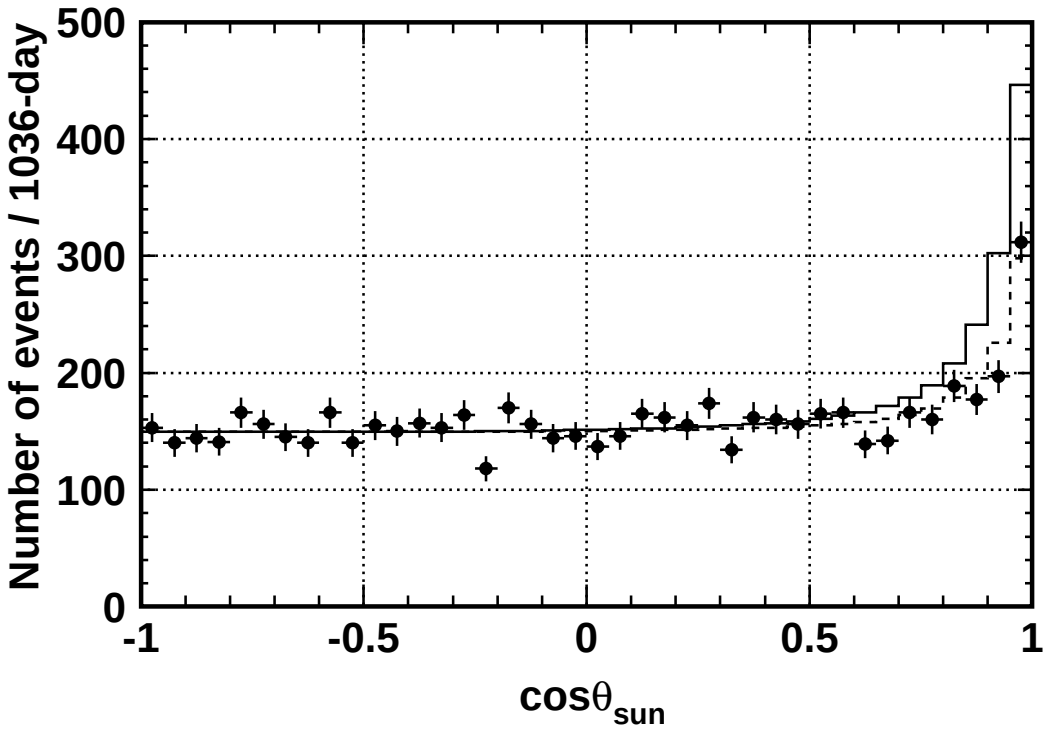

Fig. 6. Solar neutrino peak from 1036 days of Kamiokande III. The solid line histogram shows the prediction from Ref. 23, the dashed histogram the best fit to the data points.

2.2.2 Interlude: The Three Solar Neutrino Problems

Having discussed the radiochemical chlorine and gallium experiments and the Kamiokande water Cherenkov experiment, it is worth reviewing the current state of the solar neutrino problem to understand the motivations for the so-called second-generation solar neutrino experiments. Three solar neutrino problems emerged as experimental information became available. The first, a general shortage of observable flux on earth when compared to solar model predictions, came to light immediately with the first solar neutrino flux measurement by the Homestake chlorine experiment. Yet solar models at the time, i.e., before helioseismology put them to a rather stringent test, were not deemed reliable enough to make neutrino

physics the most likely explanation. Use of extrapolations from rather high-energy measurements to derive the nuclear cross sections at energies found in the solar interior was criticized.[24] Thus, even with the advent of the Kamiokande measurement, particle physics solutions to the solar neutrino problem were not widely favored. The second solar neutrino problem is that translating the Kamiokande ^{8}B flux result into an expected chlorine counting rate gives a number exceeding the chlorine measurement. Although the Kamiokande-inferred flux is only a fraction of the expected ^{8}B flux, in conjunction with the chlorine results it still leaves no room for ^{7}Be neutrinos, which are expected from the reaction in the chain that is needed to produce the observed ^{8}B neutrinos. Only after the gallium experiments both essentially failed to see any flux at all, above that expected from the fundamental proton fusion reaction, did the solar neutrino problem capture the imagination of a wider particle physics community.

The solution currently favored by most physicists' prejudice is neutrino oscillation of electron neutrinos into muon neutrinos. The varying depletion factors measured for different parts of the solar neutrino spectrum suggest an energy dependence of the suppression mechanism. The best available fit to all existing data is obtained for matter-enhanced neutrino oscillation. Specific predictions of this interpretation will be tested by the next generation of solar neutrino experiments: distortions in the spectral shape of ^{8}B neutrinos especially, and a day/night flux difference from regeneration in the Earth. Comparison of neutral and charged current event rates will directly test for a muon neutrino component in the solar neutrino flux. A dedicated measurement of the ^{7}Be neutrino flux will provide another sensitive test of proposed solutions to the solar neutrino problem as well as the overall consistency of the experimental data.

2.2.3 Super-Kamiokande

Super-Kamiokande is the successor to the Kamiokande experiment. Like Kamiokande, it provides real-time directional information on solar neutrino interactions from elastic scattering off electrons. Apart from the overall suppression of the ^{8}B neutrino flux established by Kamiokande, two signatures of neutrino oscillation observable in Super-Kamiokande certainly could not be of astrophysical origin: a possible distortion of the ^{8}B neutrino spectrum, or a difference between the day

and night fluxes of solar neutrinos. Owing to its systematic limitations Kamiokande was unable to resolve these features in its data.

Improvements in size and various aspects of the layout aim to increase the statistical precision and reduce the systematic errors with respect to Kamiokande. The basic design is a cylindrical water Cherenkov detector surrounded by an anticounter. In the solar neutrino analysis, the anticounter serves mainly as a passive shield against γ-rays from the surrounding rock. The size is increased to the largest which can be safely excavated. Sited close together in the same mine, Kamiokande and Super-Kamiokande are shielded against cosmic rays by the same mountain, and thus, share the same overburden: 1000 m of rock or 2700 MWE.

The physical dimensions of 39.3 m diameter and 41.4 m height for the stainless steel tank, and 33.8 m diameter and 36.2 m height for the inner detector (ID), correspond to a 33-fold increase in fiducial volume for the solar neutrino analysis (Fig. 7). The 22.5 kt fiducial volume begins 2 m from the ID PMT surface. 11,146 improved 20-inch PMTs cover 40% of the otherwise low-reflectivity inner surface. The inner and outer detector (OD) are separated by a light barrier of two opaque sheets enclosing 55 cm of water and a stainless steel structure on which all PMTs are mounted. The ID is therefore shielded from γ-ray activity in the surrounding rock by at least 2.6 m of water. On the outside of this light barrier, 1885 8-inch PMTs view the OD, which is lined with highly reflective white material.

The Kamiokande experiment was able to lower its analysis threshold down to 7 MeV. Even at this relatively high threshold, the main contribution to the background in the solar neutrino analysis comes from the 3.3 MeV β-decay of ^{214}Bi in the radon decay chain. To allow a sensitive test for distortions of the ^{8}B neutrino spectrum, the analysis threshold must be pushed as low as possible. For Super-Kamiokande, radon will be the major obstacle to lowering the analysis threshold to 5 MeV. The Super-Kamiokande water purification system is designed to allow a factor of 100 reduction in the radon concentration compared to Kamiokande, achieving radon levels in the tank water below 5 mBq/m^3. The water is constantly recirculated through the purification system, exchanging one detector volume in a little over a month.

Construction, filling, and calibration of the ID PMTs to achieve a uniform detector response were finished in time for the start of the experiment on April 1, 1996, 00.00 h. Another two months of recirculating the tank water were required until a steadily increasing water transparency stabilized at about 75 m (at 400 nm).

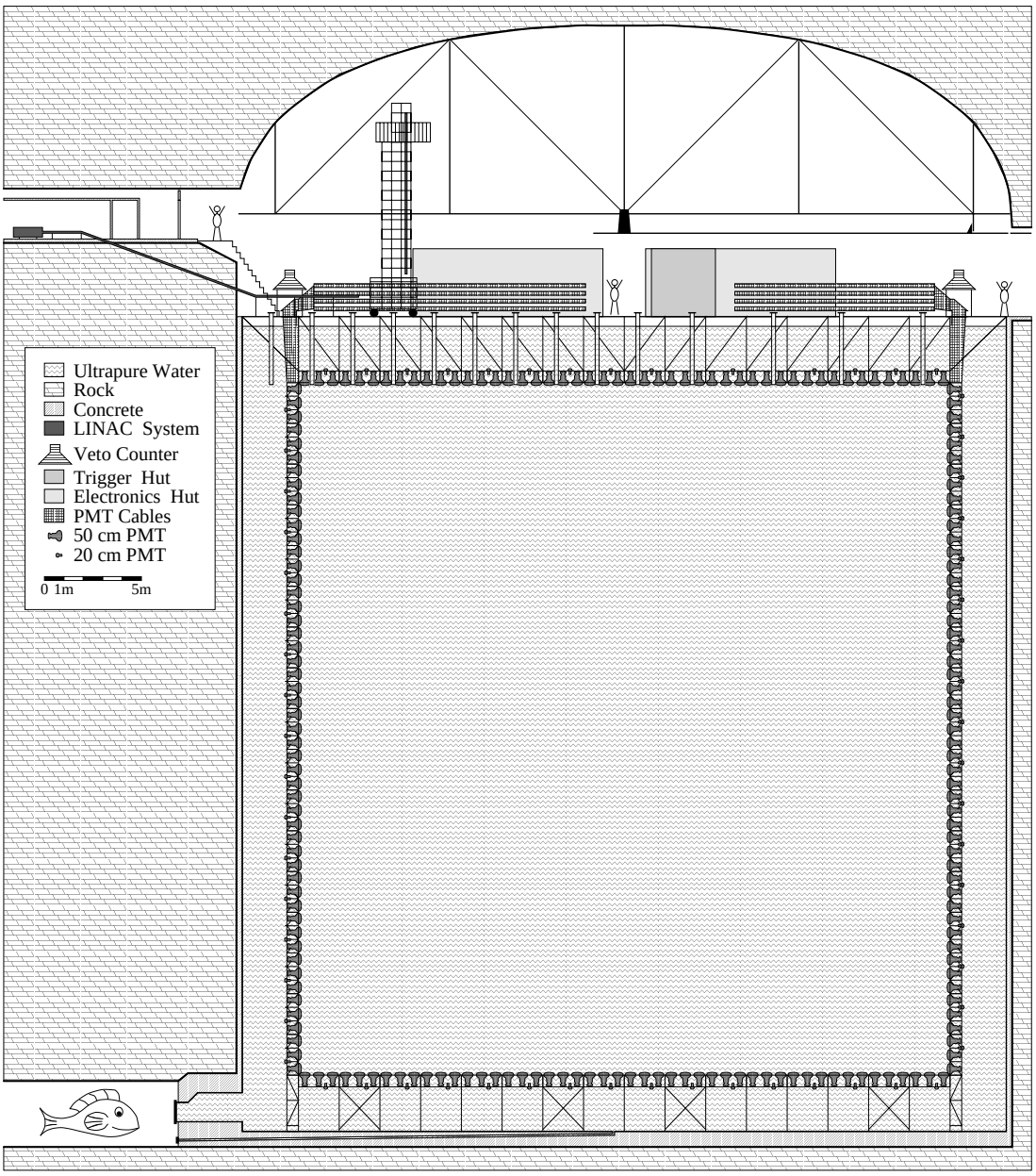

Fig. 7. The Super-Kamiokande detector.

Because of the shifts in absolute energy calibration associated with changes in water transparency, physics analysis of Super-Kamiokande data begins only at the end of May 1996. Water transparency is monitored directly from the data, and the energy calibration closely follows its changes.

PMT signals from the ID are processed in custom-made electronics which digitize the time and charge of PMT hits. The boards are self-triggering with a threshold of 1/4 photoelectron (PE) equivalent. The timing range spans 1.2 μs, with 0.3 ns resolution, and charge is recorded up to 550 pC, with 0.2 pC resolution. Charge measurement reaches digital overflow at 250 photoelectrons.

The gain of ID PMTs is adjusted with light from a scintillator ball, driven by a xenon lamp, reducing the spread in relative gain over all tubes to 7%. For timing calibration, short pulses of a nitrogen laser are diffused from the center of the ID. The average timing resolution of the inner detector PMTs is 3 ns at the 1 PE level, reaching a limit of 0.6 ns at about 100 PE.

Readout of the detector is initiated when a certain number of PMTs are hit within 200 ns. To avoid dependency of the detector trigger threshold on changing PMT noise levels, the signals are AC-coupled into a discriminator. Current trigger thresholds for the ID correspond to 29 and 31 hits, the lower one corresponding to a total energy of 5.5 MeV for electrons. The respective trigger rates are 10–12 Hz and 4.3 Hz. OD-triggers are generated independently at a rate of 2.7 Hz. A 25 hit threshold is just becoming operational in an effort to lower the analysis threshold for solar neutrinos.

To reduce the systematic errors arising from the energy scale and the angular resolution, a linear accelerator for electrons (LINAC) is installed on-site at Super-Kamiokande. It provides a low intensity beam ($\sim$ 0.1 electron/pulse) with well-defined energies from 5 to 16 MeV, thus matching the energy range of interest to the solar neutrino analysis. Intensities of significantly less than one electron per accelerator pulse are required to ensure single electron signals in the tank. The beampipe delivering the electrons to the detector can be inserted from the top of the tank at various radial positions and can be extended to various depths in the ID. Electron momenta are selected by bending the beam through a set of collimators before transporting it along the top of the Super-Kamiokande tank to the point of insertion. Calibration of the beam energy is achieved by dumping the beam into a germanium crystal, which is calibrated with a variety of γ-ray sources. Electron energy loss in the beryllium entrance window to the crystal, as

well as in its passive layers, was carefully calibrated at a suitable spectrometer. The maximum observed offset between calibrations with identical magnet settings for the beam momentum is 20 keV.

After being bent into the tank, the downward-going electrons leave the beam-pipe through a 100 μm titanium window, after passing 1 mm of plastic scintillator which provides a trigger signal. For each position in the tank, data are taken over a range of energies. To study possible background from the operation of the LINAC itself, additional data are taken at each position and energy with an artificial electron trigger. Analysis of these data show no such background, hence systematic corrections from such background must be less than 0.16% at all energies and positions. In summary, the LINAC performance fully satisfies expectations and provides a beautiful energy and angular resolution calibration for the Super-Kamiokande experiment.

It came as a surprise when it was found that the energy scale inferred from the LINAC calibration was 1.4% higher than the one previously obtained from a substantially improved nickel calibration procedure applied in Super-Kamiokande. This was problematic since Super-Kamiokande set out to control these errors to the level of 1%. Improvements with respect to the Kamiokande calibration come from the source design and the addition of a californium fission trigger. The latter allows considerable improvement in background subtraction using the 85 μs time constant for neutron capture on nickel. A thorough investigation of the nickel calibration revealed several problems related to the nickel MC simulation that brought the discrepancy down to 0.8%. Confidence in the new LINAC-based energy calibration is increased by yet another calibration based on the β-decay of ^{16}N. This isotope ^{16}N is generated throughout the detector volume by stopping muons of negative charge reacting with a proton in an ^{16}O nucleus. About 40 such reactions are expected within the 22.5 kt fiducial volume per day. The decay of ^{16}N has a Q-value of 10.4 MeV, mostly transferred to the decay electron, and a half-life of 7.13 s. Preliminary results from this calibration show excellent agreement with the new LINAC-based energy scale.

Solar neutrino results from the Super-Kamiokande experiment are described in a dedicated Super-Kamiokande lecture by Y. Itow in the Topical Conference section of the Institute. At the start of the experiment, flux measurements were made independently by the Japanese and American groups of the collaboration, each using their own analysis programs and MC, sharing only timing and charge

data of events. Despite very different background characteristics, the analyses agree well and confirm the old Kamiokande result. A possible day/night effect can neither be confirmed nor be ruled out with the present Super-Kamiokande data. To draw conclusions from the observed recoil electron spectrum in Super-Kamiokande, the ongoing reduction of the analysis threshold to 5 MeV will be crucial.

2.2.4 The Sudbury Neutrino Observatory

A heavy-water (D_2O) solar neutrino experiment had originally been planned by a group at Case Western Reserve.[25] The idea was abandoned as the upper limit of the relevant high-energy solar neutrino flux measured with the Homestake chlorine experiment turned out to be significantly lower than expected. The reaction used for neutrino detection in heavy water is not the elastic scattering on electrons used in the conventional light water Cherenkov detector, but the latter contributes to the total cross section the same way it does in the conventional detectors.

On deuterons the CC reaction $\nu_e + D \to p + p + e^-$ is observed using the water Cherenkov technique on the outgoing electron. Compared to the ES reaction, the CC reaction has a higher cross section and a much better energy correlation between the incoming neutrino and the outgoing electron: $T_e = E_\nu - Q - p_p^2/m_p; Q = 1.44\,\mathrm{MeV}$. This, together with the fact that any ν_μ or ν_τ generated by oscillation does not contribute to the signal, should make possible a more sensitive test for distortions of the ^{8}B neutrino spectrum from the sun. Yet the correlation of the outgoing electron direction with that of the incoming neutrino is much weaker than in ES: $[\sim (1 - \frac{1}{3}(p_e/E_e)\cos\theta)]$, making statistical background subtraction more difficult.

The other important neutrino reaction in a heavy water detector is NC scattering on nucleon constituents, leading to deuteron breakup: $\nu_X + D \to \nu_X + p + n$. In this reaction there is no outgoing charged lepton that can be directly detected in a water Cherenkov detector. Other means must be devised to subsequently detect the neutrons in a separate reaction, making impossible any inference with respect to the incident neutrino's energy or direction, apart from it having had at least the 2.2 MeV needed to break up the deuteron bond.

A heavy-water Cherenkov detector is currently being built in Sudbury at the Creighton Mine, Ontario, Canada. The site for SNO (Sudbury Neutrino Obser-

vatory) is 2070 m deep (6200 MWE), and thus, very well shielded against cosmic ray induced background; this is particularly important for measuring the NC reaction. 1000 t of heavy water (99.85% D_2O) are contained in an acrylic sphere of 12 m diameter, which is suspended at the center of another 14.5 m diameter spherical volume filled with clean light-water (Fig. 8). Its spherical inner surface is covered with 9600 inward-looking eight-inch PMTs. To enhance light collection, all PMTs are equipped with light collectors to bring the effective photosensitive area up to 70% of 4π. As in Super-Kamiokande, this water Cherenkov detector is surrounded by an outer detector, here equipped with $\sim$ 100 PMTs. Separate water purification systems treat the light- and heavy-water.

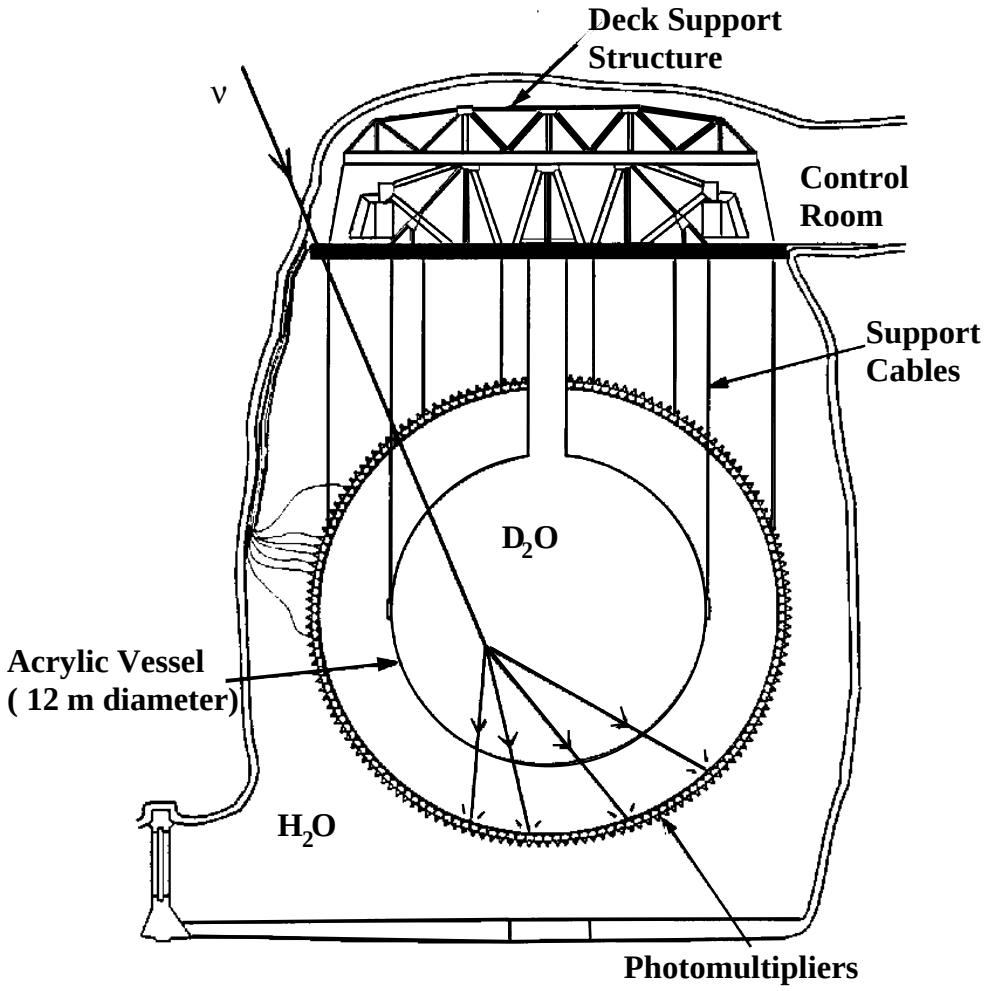

Fig. 8. The Sudbury heavy-water detector.

Two ways of detecting the neutrons produced in the NC reaction are possible. In one case, strings of ^{3}He proportional counters are suspended throughout the detector volume on a 1 m grid, to capture thermalized neutrons. Forty-two percent of the neutrons from neutrino-induced deuterium breakup should be captured on ^{3}He. Energy and risetime cuts will be used to suppress background from internal α- and β-decays in the counters. The other option is to dissolve 2 t of $MgCl_2$ in the heavy water. This gives an 83% chance of neutron capture on ^{35}Cl, after which 8.5 MeV are released from the excited nucleus into a γ-cascade. This cascade is to be detected in the water Cherenkov detector. If nothing is done to detect deuterium breakup in the detector, 30% of the neutrons will still be captured on the deuterium itself, producing γ-rays of 6.25 MeV throughout the detector volume, resulting in an expected 500 events over a 5 MeV threshold per year. Under the same BP95 flux assumptions, about 2500 events are expected for a $MgCl_2$ admixture, to be compared to about 2000 in the ^{3}He counters. Since the removal of the $MgCl_2$ is a time-consuming process, it is expected to remain in the detector for more than half a year at a time. Background to this specific reaction should be dominated by exactly the same signature produced by photodisintegration of deuterium. To avoid γ-ray activity around the detector as much as possible, stringent radiopurity standards are imposed on the materials used for the construction of the detector (including the glass of the PMTs). For the CC reaction, BP95 flux assumptions lead to a prediction of 3000 events per year over a threshold of 5 MeV; 400 events from neutrino electron scattering are also expected.

SNO is expected to start taking data in 1998. If its ability to independently measure the CC and NC contribution to the ^{8}B solar neutrino flux here on earth and to unfold the ^{8}B electron neutrino spectrum materializes, the experiment should be capable of resolving the issue of matter-enhanced neutrino oscillations on the basis of only one year's data.

2.3 Future Real-Time Experiments

The experimental techniques used to establish what is known today as the Solar Neutrino Problem and that we have encountered so far have severe limitations. Radiochemical experiments yield no information at all about important characteristics of individual events like timing, energy, or direction. The water Cherenkov

technique provides information on timing, direction, and a lower limit on the energy of the neutrino derived from the energy of the recoil electron in the elastic scattering process, but is limited to relatively high energies and renders charged and neutral current events undistinguishable.

As the first of a variety of future experiments seeking to overcome these limitations, SNO features an enhancement of the classical water Cherenkov technique that should allow separation of CC and NC contributions to the neutrino interaction rates.

Just as for huge water Cherenkov detectors, light output can easily be measured at the surfaces of large liquid scintillator volumes. Scintillation light overcomes one of the water Cherenkov limitations by providing high light yield down to low-energy experimental signatures; however, it has the clear drawback of losing all directionality that a specific reaction employed in the experiment might provide. Yet sensitivity to low-energy events in the detector usually incurs high trigger rates, and a rapidly deteriorating signal-to-noise ratio from both environmental and intrinsic radioactive backgrounds. The lack of directionality, which in water Cherenkov detectors allows for a highly effective statistical background subtraction, clearly aggravates this problem. Extremely high radiopurity levels for materials in and around the detector volume are mandatory. Another way out of this problem may be possible via delayed coincidence techniques, if the reaction under study leads to excited states of suitable energy, lifetime, and de-excitation mechanism in the product nucleus.

Electronic measurement of individual charged particle tracks emerging from a neutrino interaction is now possible in large volumes of liquified or highly pressurized noble gases. This approach, slightly reminiscent of bubble chamber techniques, clearly gives the most detailed information on individual events.

2.3.1 Borexino

The name of the Borexino experiment is for historical reasons. Borex (Boron Experiment) was intended to become a 2-kt liquid scintillator experiment loaded with boron to allow measuring of the CC and NC reaction rate of ^{8}B neutrinos.[26] Borexino was to be a 100-t test bench to verify its feasibility. In 1989 the focus shifted upon the realization that, with the low-background techniques required for Borex, elastic scattering of ^{7}Be neutrinos might already be measurable with

a plain scintillator in this smaller detector. The boron was dropped from the proposal and a 100-t liquid scintillator experiment operating in the energy region between 250 and 750 keV became the new Borexino experiment that is currently being built at the Gran Sasso laboratory in Italy.

Relying on scintillation light for detection, the directionality provided by elastic scattering is lost as a means of identifying solar neutrino events. The ^{7}Be neutrinos will be identified by a Compton-like edge at about 660 keV in the spectrum. Statistical subtraction of the background spectrum will yield the flux of these neutrinos. Should the flux predicted by BP95 be observed, the expected event rate will be $50\,\mathrm{d}^{-1}$. In the event of full conversion of this flux to either ν_μ or ν_τ, this figure goes down to about $10\,\mathrm{d}^{-1}$. If the CC event rate can be extracted from radiochemical data, this will give powerful constraints on oscillation parameters. Real-time capability allows one to look for a day/night effect and seasonal variations. The fact that ^{7}Be neutrinos are monoenergetic will allow an especially sensitive test of vacuum oscillation parameters.

Borexino will contain its 100 t of liquid scintillator in a spherical volume at the center of a spherical detector (Fig. 9). The outer stainless steel water tank of 18 m diameter contains a stainless steel sphere of 13.7 m diameter, which confines the detector volume. On this sphere 2200 inward-looking eight-inch PMTs collect the scintillation light and 200 outward-looking PMTs collect Cherenkov light from entering charged particles. The inside of this assembly will be lined with a nylon film to suppress radon diffusion into the detector volume. Another nylon sphere of 8.5 m diameter will be suspended at its center and contain the liquid scintillator. The volume between the nylon sphere containing the liquid scintillator and the nylon barrier lining the inner steel sphere will most likely contain the organic liquid that is used as scintillator solvent, eliminating problems with buoyancy and changes in refractive index at this internal surface. Eighteen hundred of the inward-looking PMTs will be equipped with light cones to enhance light collection from the scintillator sphere, while 400 will be bare to also collect Cherenkov light emitted by particles passing through the scintillator-free solvent. The effective photocathode coverage of the inner detector surface will be 35%.

Natural radioactivity has to be the paramount concern in an experiment which aims at recording all low-energy activity over a vast volume. Three "thresholds" exist, at each of which problems with the radioactive background intensify significantly. At about 5 MeV ^{208}Tl in the decay chain of ^{232}Th and ^{214}Bi in the decay

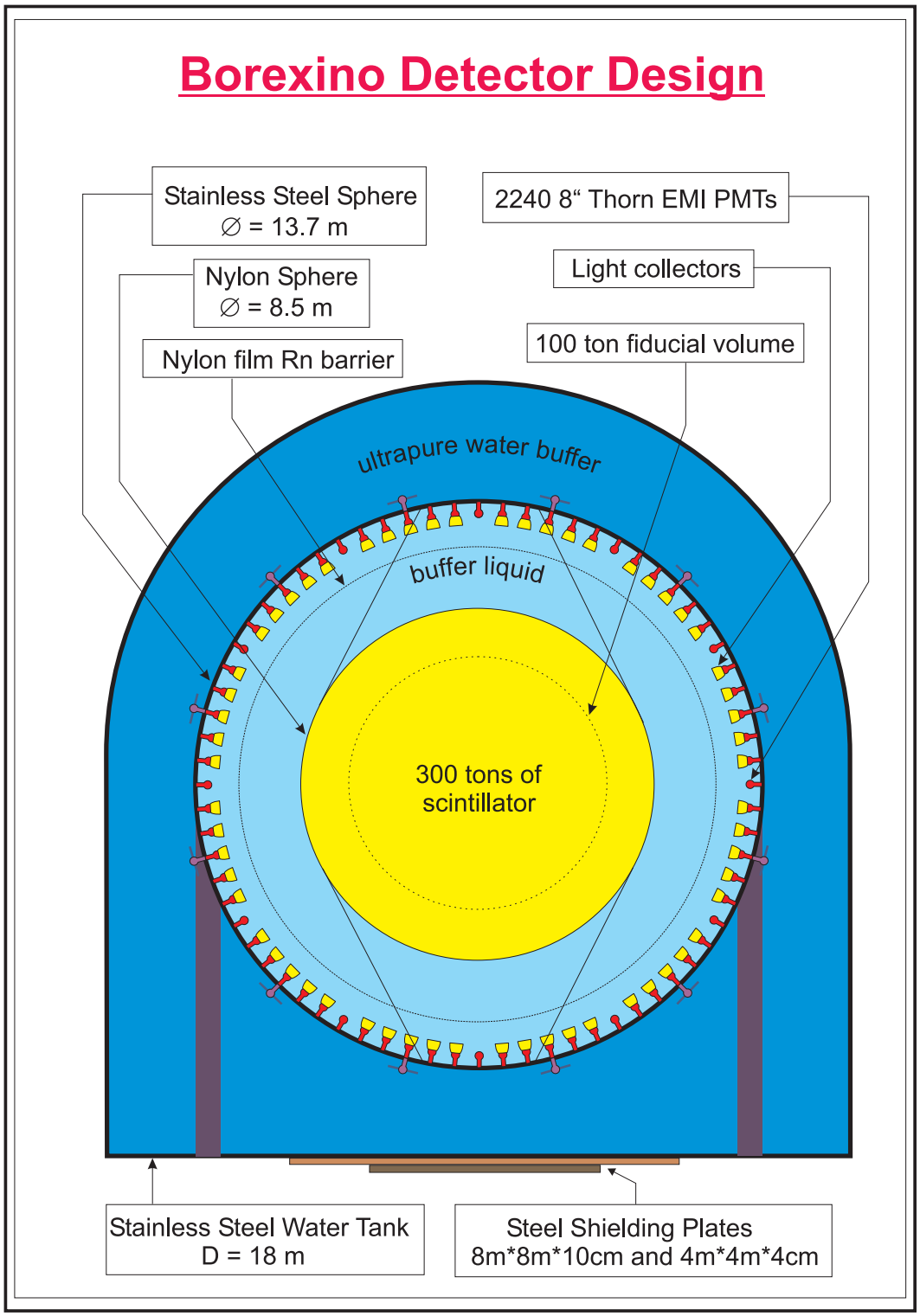

Fig. 9. The Borexino detector.

chain of ^{238}U and ^{222}Rn starts to hurt. At about 2 MeV ^{40}K sets in, and below 250 keV the decay of ^{14}C has to be the major concern. Borexino plans to meet these challenges with a strategy called graded shielding. The detector is designed to provide an ultra-low radioactivity environment mainly throughout its sensitive volume, the liquid scintillator. As detector elements become more and more removed from this innermost part, requirements for the radiopurity of components can be relaxed accordingly.

In the organic solvent to be used for the liquid scintillator, metals like uranium, thorium, or potassium are practically not soluble. It is synthesized from petroleum that was in underground storage for millions of years, so that ^{14}C will mostly have decayed. All PMTs are manufactured from specially selected low-radioactivity glass and mounted through holes in the stainless steel sphere, so that their cables will all be outside of this sphere. The surface of this inner steel sphere will be electropolished to facilitate a thorough cleaning from radioactive dust after construction. The two nylon barriers will slow down diffusion into the fiducial volume of radon emanating from internal surfaces. Finally, the water in the outer tank, which is highly purified to remove dust and radioactive contaminants, serves as a shield against γ-rays from the surrounding rock.

Shielding from cosmic rays is provided by a rock overburden of 3400 MWE at the Gran Sasso Laboratory. The residual muon flux of $\sim 1\,\mathrm{m}^{-2}\mathrm{h}^{-1}$ at the detector site will be tagged by its Cherenkov signal in the water surrounding the steel sphere and in the solvent surrounding the scintillator sphere, to suppress subsequent spallation events in the scintillator. Yet cosmic rays do pose a problem for Borexino's strict radiopurity requirements: the liquid scintillator materials will build up long-lived cosmogenic radioactivity (especially ^{14}C) while being prepared and treated in ground-based facilities.

To check the feasibility of the experiment, a Counting Test Facility (CTF) was built close to the Borexino site at the Gran Sasso Laboratory.[27] Since radiopurity levels required in the Borexino experiment can no longer be measured with conventional methods, this prototype detector is used to verify background levels in the scintillator material and explore possible purification techniques. A nylon membrane of 0.5 mm thickness and 2 m diameter holds the scintillator at the center of a cylindrical water tank of 11 m diameter and 10 m height. In the CTF the scintillator is viewed by 100 of the eight-inch PMTs. After the successful conclusion of this experiment, Borexino is now being built, while CTF is being

prepared to be used as a monitor for the radioactivity level of the scintillator to be filled into Borexino.

Data taking with Borexino is scheduled to start in the fall of 1999. Optimists hope that the much weaker pep neutrino line can also be seen with this experiment, although most deem that impossible.

2.3.2 ICARUS

ICARUS is planning to expose a large volume of liquid argon in a time projection chamber (TPC) to image neutrino and other rare events. The experiment will be located at the Gran Sasso laboratory in Italy. The TPC will provide three-dimensional imaging for ionizing events with mm-scale resolution.

The reactions employed in a liquid argon solar neutrino experiment are twofold: An inverse β-decay reaction on ^{40}Ar (natural abundance 99.6%) yields ^{40}K, in a CC reaction that hereafter will be referred to as neutrino absorption. Since the half-life of ^{40}K is 1.3×10^{9} y, its subsequent β-decay (mainly to ^{40}Ca) can neither be used to tag the initial neutrino reaction, nor does it constitute significant background to the experiment. A significant contribution to the neutrino absorption cross section comes from a transition to the isotopic analog nuclear state in ^{40}K, lying 4.4 MeV above the ground state.[28] Several transitions to lower-lying states are expected to be responsible for about 2/3 of the total cross section, if a threshold of 5 MeV is imposed on the recoil electron energy. Thus, γ-rays from nuclear de-excitation will accompany the CC signal, for which the recoil electron has a good correlation in energy but a rather weak one in angle to the incoming neutrino. The other reaction relevant to solar neutrino detection in the ICARUS experiment is neutrino electron elastic scattering, which through its NC contribution is sensitive to ν_μ and ν_τ as well. As mentioned before, this reaction has a good angular correlation, while the recoil electron's energy may take on any value essentially up to the incoming neutrino's energy.

The use of liquefied noble gases in large TPCs is made interesting by an energy resolution of a few percent in the MeV range, combined with a spatial resolution of a few hundred μm. High drift velocities prevent pile-up of events, even if the ionization charge has to be drifted over long distances. Argon is a widely used cryogenic liquid, therefore readily available in large quantities at an affordable price. The usual avalanche amplification of the ionization signal at the sense wires,

as is used in traditional gas-filled TPCs, is not available in liquid noble gas filled devices. Thus, the detectable signal is very small, since 1 mm of minimum ionizing track produces only up to 10^4 electrons. Moreover, depending on the strength of the drift field, a significant fraction of the primary ionization produced along the track will be neutralized by recombination. And while the high density of liquid argon is a boon in terms of target mass, it may constitute a problem for signal collection if trace impurities with the capacity to adsorb the drifting electrons are present. The high collision rate for the drifting electrons in the liquid will then result in high attachment rates and decrease the signal along its path. Thus, stringent requirements for the purity of the liquid argon are mandatory. For a system big enough to provide the fiducial masses required in neutrino experiments, thermal stress imposed on delicate detector components when cooling it to liquid argon temperature after construction, or reheating it for maintenance, also has to be given serious consideration.

On the way to a 5-kt liquid argon detector for the ICARUS experiment, the first 600 t module will offer 360 t of sensitive mass for solar neutrino observation (Fig. 10). Height, width, and depth of the inner volume of the stainless steel dewar will be $3.7 \times 7.3 \times 18\,\mathrm{m}^3$. The dewar dimensions are chosen to fit through the tunnels at the laboratory, since the module will be assembled and tested outside of it. The inner volume will be divided into two halves by a vertical wall running parallel to the longer of its outer walls. A TPC field cage will be fitted into each of the halves, dividing its respective volume into two drift regions. Electrons drifting in one of the two halves will move horizontally from a central cathode towards counting regions mounted on the long sides of the dewar and on the central wall dividing the dewar. The maximum drift length is 1.64 m, corresponding to a drift time of about 1 ms at a typical strength for the drift field. The pitch of the wire chambers will probably be 3 mm, with successive sense wire planes reading the coordinates perpendicular to the drift direction. Since no amplification can be done, the signal is read nondestructively from the current induced by the passing ionization charge. The signal induced on the first wire plane starts as soon as charges are produced in the drift volume, providing a start for the drift time measurement. Signal duration on later wire planes is limited by shielding through the adjacent wire planes. Increasing the electric field strength between subsequent wire planes prevents charge from being collected on the wires. Various alternative

solutions for the design of the wire planes are currently being considered. Self-triggering circuitry will allow the detector to be continuously sensitive.

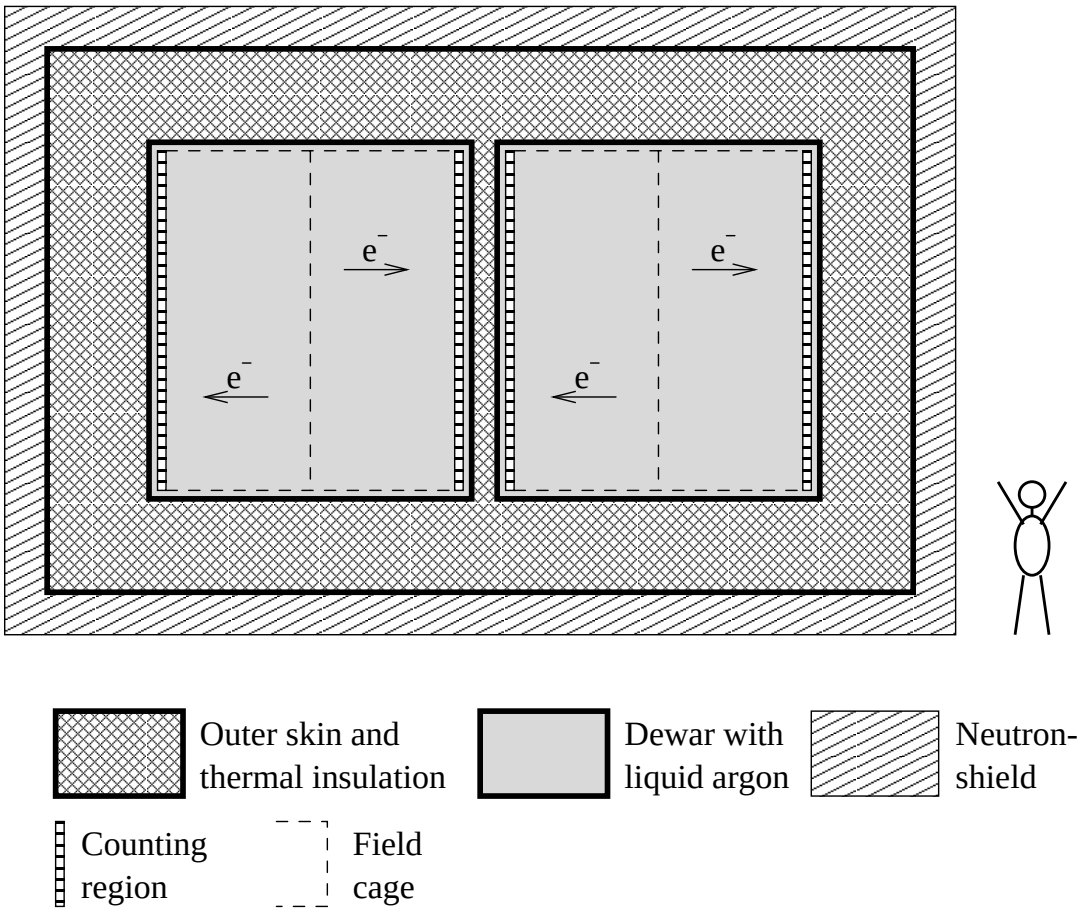

Fig. 10. Cross section of the planned 600-ton ICARUS module. This figure is inspired by a three-dimensional sketch of the ICARUS detector posted at http://www.aquila.infn.it/icarus.

A 3 t prototype detector,[29] operated since May 1991, verified the fundamental design parameters and the stability of detector operations.[30] Results from experimentation with this prototype show that the problem of losing charge to recombination can be alleviated by doping the argon with tetra-methyl-germanium (TMG).[31] In the recombination process, photons are emitted with typical energies matched to the photoionization potential in TMG. Moreover, photons from excitations produced along the track of the ionizing particle can thus be converted to enhance the measurable charge recovered in the detector. Dopant concentration levels have to be sufficiently high to limit the spread of this charge conversion

to the wire pitch in the chamber. The addition of TMG to the liquid argon in the prototype detector resulted in a significant improvement in the linearity of the dE/dx measurement (particle ID), without compromising the stability of detector operation.

Background to solar neutrino observation in the ICARUS experiment is expected from radioactivity mainly in the detector surroundings. With radon condensing at temperatures significantly higher than that of liquid argon, this major contribution to the backgrounds in other ^{8}B solar neutrino experiments plays no role here. Background intrinsic to the detector is presented by the β-decay of ^{42}K (half-life 12 h, endpoint energy 3.5 MeV) in the ^{42}Ar (half-life 33 y) decay chain. ^{42}Ar is found in natural argon as a contamination at a level $< 10^{-21}$. Owing to the excellent calorimetric properties of the detector, the quoted decay is deemed insignificant as source of background at that level of contamination. Since choices for detector materials will depend on the detector design, stainless steel is the only structural material considered so far, and batches of the required radiopurity seem commonly available. Gamma-rays from radioactivity in the surrounding rock are expected to contribute a significant amount of electron tracks through Compton scattering. According to simulations, the energy of these electrons is limited: No tracks were found to have an energy in excess of 2.4 MeV. Given the energy resolution of the detector, the probability for such electrons to fake a 5 MeV track is $< 10^{-6}$; i.e., practically no triggers are expected from that background. At the estimated level, these Compton electrons are also not expected to interfere with the identification of absorption events through low-energy activity associated with the main trigger. The most significant background to the trigger rate above 5 MeV is that expected from neutrons thermalized and captured near the detector, the capture being followed by higher energy γ-emission. Without further shielding, most of the neutrons would be captured in the stainless steel dewar. A neutron shield will therefore surround the whole detector module. Using boron as a component in this shield for neutrons to get captured on, will result in significant softening of the resulting γ-spectrum.

With the planned threshold of 5 MeV on recoil electron tracks, assuming an unabated BP95 ^{8}B solar neutrino flux interacting in a sensitive volume of 360 t, the expected solar neutrino event rate for one year comprises 330 events from elastic scattering, 610 from absorption to the low lying states, and 285 from absorption to the isotopic analog state. Apart from the rate suppression already seen in other

experiments, cuts applied in the actual analysis will claim their toll on these numbers. First efficiency estimates for such cuts, based on detector simulation, were presented alongside the numbers quoted in Ref. 32.

The addition of 5% of deuterated methane would allow one to exploit the superior resolution of the ICARUS detector for the CC reaction used in the SNO experiment. This proposition is currently being evaluated.

2.3.3 HELLAZ

An attempt to measure the p-p neutrino spectrum will be made in the HELLAZ (HELium at Liquid AZote [French for nitrogen] temperature) experiment. In a cylindrical TPC of 11 m diameter and 20 m length, 6 t of He at liquid nitrogen temperature and five-bar pressure will offer 2×10^{30} electrons as target for the elastic scattering reaction. Alternatively, the TPC could be operated at a temperature of 150 K and ten-bar pressure. The experiment is planned for the Gran Sasso Laboratory in Italy.

In elastic scattering the incident neutrino energy can in principle be reconstructed kinematically if the direction and energy of the recoil electron are determined with adequate accuracy and the neutrino is assumed to be coming from the sun. In a drift chamber the kinetic energy of a particle, the track of which is contained in the detector, can be inferred from the amount of ionization produced along that track. Optimal use of this information can be made if this charge is counted in its fundamental units, the electron charge. If this can be achieved, energy resolution on the recoil electron will only be limited by statistical fluctuations in the number of electrons produced along the track. In a HELLAZ-type TPC the uncertainty in the incident neutrino energy will then be dominated by the angular resolution of the reconstructed electron track. With an anticipated threshold of 100 keV on electron energy, tracks will at least be 5 cm long. Although helium is almost optimal with respect to multiple scattering, only the first 10 mm of the track should be used to determine the direction, requiring high spatial resolution throughout the fiducial volume. With an anticipated uncertainty in the recoil electron energy of order 3% (about double the limit derived from counting statistics in an appropriately quenched mixture), and of 35 mrad for the angular resolution, the error in the energy of a 300 keV incident neutrino will be less than 4%. This error will increase by roughly a factor 2.5 at neutrino energies around

860 keV, the energy of the higher ^{7}Be line. It is hoped that one can decompose the flavor mix of pp neutrinos arriving at the Earth by means of the different recoil energy distributions for ν_e and $\nu_{\mu,\tau}$.[33] If pure CF_4 were used as the counting gas, the angular resolution would become worse by a factor of two, but a CC reaction on ^{19}F with a threshold of 3.25 MeV could be used for ^{8}B neutrino detection.

The cylindrical TPC will be divided into two halves by a central cathode (Fig. 11). Electrons are drifted horizontally towards the two detection modules of 11 m diameter at the cylinder endcaps. An alternative design of rectangular prismatic shape is also under discussion. The TPC will be shielded by 2.5 m of solid CO_2. The containing stainless steel pressure vessel and its thermal insulation are surrounded by a neutron shield.

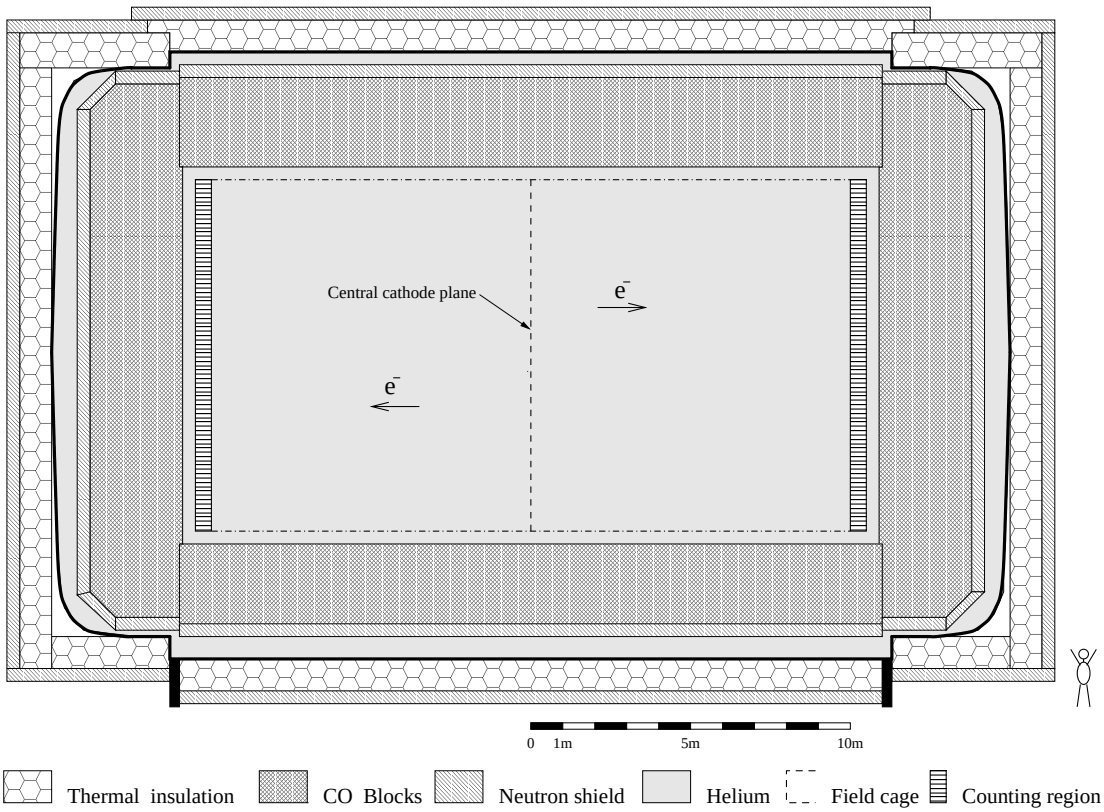

Fig. 11. Cross section of the HELLAZ detector. The figure is inspired by a figure in the preprint CERN-LLA/94-19.

Background radon will not cause a problem, because, as in the ICARUS detector, it is immobilized by the low temperature. With an anticipated threshold as low as 100 keV, essentially all radioactivity or radiation entering the TPC will

cause triggers. Fortunately, the target material itself is radiopure and will not cause problems as long as the quencher needed for wire chamber operation does not introduce one. Radioactivity inherent to structural materials bounding the sensitive volume of the TPC cannot yet be known, but has to be controlled as tightly as possible. Major quantities of stainless steel will only be outside of a shield of solid CO_2, which itself is far enough from the sensitive volume to eliminate concerns about its ^{14}C. Shielding against γ-rays and neutrons from the surrounding rock is the most serious background problem the detector is deemed to face. Replacing the CO_2 shield with a shield of B_2O_3 would increase the local density in the shield and, being solid at room temperature, would significantly facilitate the construction of the detector, but the availability of this material at the required level of radiopurity still has to be proven.

Amplification at the counting wires cannot be controlled in pure helium; addition of a quencher is needed. The choice of the right counting gas mixture is heavily constrained by the requirement to achieve single electron counting. A slow drift clearly helps to translate spatial separation between drifting electrons into time available to separate successive hits on a single wire. Yet in a traditional wire chamber, slow drift and the fast counting required to avoid overlapping of signals from successive hits are almost contradictory requirements. Signal duration is linked to the time it takes to absorb the positive ions from the avalanche on the cathode, a process generally delayed by a slow drift.[‡] This problem can in principle be solved by reducing the distance over which the avalanche develops. Thus, a microgap chamber[34] rather than a conventional wire chamber might be a sensible choice as the actual detector in the HELLAZ TPC. A design using an electrostatic demagnifier to image a sizable section of the detector onto the submillimeter structures of a microgap chamber also involves two so-called gas electron multipliers. These structures allow a fast amplification of a factor of 1,000 each before the signal even reaches the microgap chamber. Experimental studies are in preparation.

Options for a suitable quencher were investigated in a small test TPC equipped with a multiwire chamber allowing two-dimensional readout through cathode strips.[35] A standard choice is CH_4, which has the drawbacks of slightly worsening the multiple scattering and introducing ^{14}C into the detector volume, and

[‡]Although electron and ion mobility are not the same quantity.

was shown to produce increasingly slower signals as the pressure was increased in the test TPC's conventional wire chamber. The admixture of hydrogen gas as a quencher offers some clear advantages: It enhances the detectable electron signal from charged particle tracks (by converting UV photons into more electrons) more efficiently than CH_4, introduces no radioactivity, and does not add to multiple scattering. Yet it requires additional safety regulations, especially in a confined underground environment, and did not show a suitable plateau for single electron counting in the test TPC. The quencher will have to be admixed to the helium at the level of 1%.

On the way to an installation of the full 2000 m^3 detector, two more intermediate steps are planned: Over the years 1998–99, a 2 m^3 TPC will be constructed and employed to determine experimentally an energy resolution function for neutrino electron scattering from Compton scattering induced by a radioactive γ-source. Subsequently, a 40 m^3 HELLAZ prototype will be built and installed at Gran Sasso before the year 2002 to verify the shielding and measure the background from radioactivity *in situ*.

2.3.4 HERON

Using superfluid ^{4}He as a target material for neutrino electron elastic scattering at the lowest energies is another proposal towards direct pp neutrino detection.[36] Phonons and rotons excited in the superfluid phase by the electron recoiling from the neutrino interaction will at sufficiently low temperatures propagate ballistically, i.e., without attenuation or scattering, over long distances. Impact on a free surface of the liquid will result in burstlike evaporation of atoms from the surface. A bolometric device suspended above the surface will react to the adsorption of these atoms with a sudden rise of its temperature. The magnitude of this rise in temperature is correlated with the energy deposited in roton and phonon excitations by the recoiling electron.

With 10^3 to 10^4 such bolometers reading out a total mass of 10 t of superfluid ^{4}He, an expected rate of 20 events per day from pp neutrinos seems possible above a threshold of ≤ 10 keV.

Recent measurements with α-particles stopping in superfluid helium find anisotropy in roton propagation with respect to the track direction, suggesting that directional measurements might be possible in such a detector.[37]

2.3.5 CC for pp Neutrinos

Real-time detection of solar neutrino induced inverse β-decay reactions by means of detecting the associated outgoing electron does not seem a viable option at low energies: Scintillation counters with thresholds low enough to detect pp neutrino induced transitions would inevitably incur prohibitive background rates from all kinds of sources. Yet there may be a way around this problem if the inverse β-decay reaction involves excited states of the product nucleus that would provide leverage for the application of coincidence techniques. A notorious example of such a reaction would use ^{115}In as target material. Natural indium consists of 95.7% of the target isotope, and inverse β-decay populates an excited state of ^{115}Sn with a half-life of 3.3 μs, ideally suited for a delayed coincidence. The threshold for neutrino detection is only 125 keV. De-excitation from the populated isomeric state proceeds electromagnetically in two steps, emitting γ-rays or electrons of 614 keV and 498 keV respectively. The fact that the energy released in this de-excitation is much higher than the energy required in the inverse β-decay reaction already hints towards the snag coming with all these obvious advantages: With a half-life of 5.1×10^{14} y, ^{115}In itself β-decays to the ground state of ^{115}Sn, releasing 486 keV in the process. Yet a cellular detector design limiting the amount of indium per cell, and therefore the random coincidence rate incurred from its decay, while still containing the 498 keV γ-rays (only 6×10^{-3} electrons) emitted in the second step of the de-excitation process of the product nucleus, should be able to circumvent this problem. Yet since this technique was first proposed in 1976,[38] 20 years of rather intense experimental effort to implement this beautiful idea has failed to produce an actual experiment.

The same 20 years later, a new class[39] of low threshold inverse β-decay target candidates suitable for the delayed coincidence technique has again been proposed by the same author, R. S. Raghavan. Double-β-decay candidates are nuclei where the would-be β-decay product is itself β-unstable, but the ground state energy of the double-β-decay candidate is lower than that of its would-be product. In this configuration direct decay through two successive β-decays is prohibited by energy conservation and the rest-mass difference between the target nucleus and the intermediate nucleus is fairly low, as is required for a low neutrino detection threshold. Owing to the relatively long lifetimes of the respective isotopes, the subsequent β-decay of the nucleus produced in the neutrino interaction cannot

be used in the coincidence. As with the indium experiment, one has to exploit transitions involving excited nuclear states of the product nucleus. In the case of ^{176}Yb, electron neutrino detection would become possible above a threshold of 301 keV, albeit with an as of yet unknown cross section. The signature to be exploited in the coincidence is a 71 keV γ or electron from nuclear de-excitation, emitted with a time constant of 50 ns. Techniques for loading liquid scintillator with ytterbium on the scale needed for neutrino experiments are available. Some spatial resolution will be needed to suppress random coincidences. The cross section will be extracted from the forward-scattering cross section in (p, n) reactions, which is currently being measured.

3 Atmospheric Neutrinos

Atmospheric neutrinos are created by weak decays of secondary particles from cosmic ray showers in the Earth's atmosphere. Thus, their energy spectrum and flavor composition depend on the composition and energy spectrum of the beam (cosmic rays) and target (atmosphere). The primary source of atmospheric neutrinos is the decay of mesons, especially charged pions and kaons, and of muons created in the meson decays. The spectrum of charged primary cosmic rays has a cutoff at lower energies imposed by the Earth's magnetic field, which is in turn modulated by solar activity through the solar wind.

Atmospheric neutrino detectors are typically located 1–2 km underground. Therefore, the distance between a neutrino's origin and the detector varies with the zenith angle. This variation ranges from about 10 km, which is the height above ground where the bulk of the neutrinos are created, up to the diameter of the earth, roughly 1.3×10^4 km.

3.1 Theoretical Expectations

Two main sources of uncertainty hamper predictions of the atmospheric neutrino event rate. Large discrepancies (of order of 25%) in the predicted fluxes of atmospheric neutrinos still exist between different calculations, and nuclear effects in the targets for atmospheric neutrino interaction obscure the experimentalists' view of what is actually going on in their detectors. The following two subsections will discuss the sources of these limitations.

3.1.1 Flux Calculations

Mesons created in hadronic interactions of cosmic ray particles on light nuclei in the upper atmosphere are the source of atmospheric neutrinos. In calculating[40–42] the expected flux, four fundamental ingredients are needed: composition and energy spectra for the primary cosmic ray particles, the target nuclei for this particle beam, interaction cross sections between the two, and finally the weak decays that produce the observed neutrinos. The problems lie with the first and third items on this list.

Composition of the primary cosmic ray flux changes slightly with energy. Measurements of the primary cosmic ray fluxes have a quoted uncertainty of about 15%. At the low-energy end of the spectrum, the geomagnetic field cuts off particles that fall below a certain threshold. This cutoff depends on position and direction, and through the geomagnetic field it is modulated by solar activity. These effects are taken into account in the calculations.

MC simulation of nuclear interactions is used to obtain the relevant spectra of the secondary pions and kaons produced. These MC models are tuned to describe accelerator data in the range of 10–100 GeV. An unsolved problem remains in the secondary pion spectra at $x_F < 0.2$ (x_F = Feynman x), where there is no data available.[43] The uncertainty introduced in the neutrino flux calculations through the nuclear collision simulation is estimated to be 10%.

Most of the sources of uncertainty in the flux calculations cancel out in the ratio of the expected fluxes of muon and electron neutrinos. An overall uncertainty in the flux normalization, typically quoted to be of order of 20%, is reduced to 5% in the flavor ratio. Thus, the atmospheric neutrino anomaly is always formulated in terms of this ratio.[44] If they were more accurately known, the absolute fluxes would allow determination of whether an observed effect is due to disappearance of muon neutrinos or appearance of electron neutrinos, answering the question of which oscillation is responsible for the effect: $\nu_\mu \to \nu_\tau$ (or $\nu_\mu \to \nu_s$, ν_s denoting sterile neutrinos), or $\nu_\mu \to \nu_e$.

Recently, data on muon fluxes at different depths in the atmosphere have become available from balloon experiments. These data are used to test the neutrino flux calculations through their predictions for the muon fluxes. It is found that the data are well reproduced by the calculations.

3.1.2 Neutrino Cross Sections

While theorists develop semiempirical approaches to model the hadronic interactions of nuclei impinging on the high atmosphere, it is mostly the experimentalists themselves who must try to incorporate nuclear effects in the description of interactions in their detectors. At energies relevant for atmospheric neutrino interactions, elastic scattering off the electrons in the target material is already suppressed by a factor of more than 10^4 with respect to the nuclear cross sections.

Experimental considerations determine the final states selected for an analysis of rate and flavor composition of the observed interactions. NC interactions do not give flavor-specific signatures, thus actually constituting background to an analysis of the atmospheric neutrino anomaly. In the CC reactions the outgoing lepton carries the flavor information from the incoming neutrino. With iron and water being the materials of choice for nucleon decay experiments, at least 89% of the target nucleons are bound in nuclei. Since shell models become too complex at energies relevant to atmospheric neutrino observation and for nuclei of mass number greater than 16, a "Fermi gas model" usually is employed to calculate cross sections in the nuclear environment. These calculations can be checked against bubble chamber data, which are well reproduced for interactions with and without associated production of pions.[45] In quasi-elastic (CC and NC) reactions, no additional particles are created apart from a recoiling nucleon. In water Cherenkov detectors especially, where recoiling protons from quasi-elastic interactions of atmospheric neutrinos mostly stay below the Cherenkov threshold (1.4 GeV), this allows unambiguous identification of the single charged track emerging from an interaction as the outgoing lepton from a CC reaction. Since the appearance of additional tracks in the detector gives rise to confusion as to which track—if any—is the lepton track carrying the relevant flavor information, often only the single track events are selected for the flavor analysis. This simple selection scheme, one charged track, which is assumed to be the lepton from a CC quasi-elastic interaction, in fact allows extraction of very clean samples, with a low NC contamination of about 5% for the muon-like events and 15% for electron-like ones.

Note that lepton universality tends to cancel out effects from mistaken cross-section estimations if experimental results are presented in the form of ratios of lepton flavors.

3.2 Experimental Situation

Two important aspects of nucleon decay and neutrino interactions are rather similar: the events are rare and no visible incoming particle initiates the interaction. The first aspect dictates a huge mass in a continuously sensitive volume, located in a well-shielded place. The second requires the ability to veto incoming particles that emerge from the shielding. Shielding against cosmic rays thus implies an underground site. For proton decay and atmospheric neutrinos, the energies are high enough that background from radioactivity is no longer a serious problem.

In the quest for proton decay (predicted by grand unified theories in the early '80s), several large-scale proton decay experiments were built. Inevitable backgrounds to their searches were the interactions of atmospheric neutrinos. In 1986, the IMB experiment published a paper remarking on missing muon decays in their data.[46] Two years later the Kamiokande proton decay experiment was the first to indicate serious disagreement between the predicted and observed ratio of muon-type to electron-type atmospheric neutrinos.[47] Although it was later realized that the initial flux calculations used to analyze these data were flawed by not taking into account the polarization of cosmic ray muons,[48] the anomaly persisted in improved analyses.

Three different signatures are relevant to atmospheric neutrino observation: fully contained events, partially contained events and upward-going muons, typically representing neutrino energies in the range of $\sim$ 1 GeV, 5–10 GeV, and 100 GeV, respectively. The first two categories are the exclusive domain of proton decay experiments.

In fully contained events, no particle or track is observed entering or leaving the detector. Within the limitations of the detector technology, these events can be fully reconstructed.

In partially contained events, one or more tracks are allowed to leave the detector from a contained interaction point. With energy loss in water of 250 MeVm^{-1}, muons from atmospheric neutrino interactions at higher energies often have sufficient range to leave the detector. Since they are the only penetrating charged particles, partially contained events are attributed to muon neutrino interactions. MC simulation asserts that this is correct at a level of $> 95\%$. The energy of the outgoing muon cannot be measured.

These first two kinds of events are only observed in proton decay experiments, as these are sensitive throughout their volume to allow for a full kinematic reconstruction of proton decay candidates. The first section of the discussion of experiments on atmospheric neutrinos is therefore devoted to proton decay experiments.

The third category—upward-going muons—can be observed in any detector that is able to discern upward-going tracks from downward-going ones. Since not even the highest-energy muons can penetrate the "length" of the earth, upward-going muons must come from muon neutrino interactions in the earth underneath the detector. Upward-going muon measurements will be discussed in a separate section.

3.2.1 Proton Decay Experiments

Fully-contained events are well described by their name: they are events for which no visible tracks enter or leave the detector volume. Unless physics considerations implicitly limit the acceptance through some trigger logic, only detector size and resolution determine the energy range accessible to a specific detector. Depending on the position and direction of a specific event, muons above a certain energy can no longer be contained. Electrons produced by an electron type neutrino, however, initiate an electromagnetic shower in the detector, and thus remain contained up to much higher energies. To allow comparison of event rates for muon-type and electron-type events over a larger energy range, partially contained events are included in the analysis.

Underground detectors normally are not magnetic, thus lacking the ability to identify the sign of the charge producing a signal in the detector. Hence, while showering electrons can be distinguished from penetrating muons by the event patterns, no judgment can be made of whether an interaction of a specific flavor was initiated by a neutrino or an antineutrino. Predictions are expressed in terms of lepton flavor, lumping together leptons and antileptons. In our discussion of atmospheric neutrinos, ν_e actually means $\nu_e + \overline{\nu}_e$ and ν_μ means $\nu_\mu + \overline{\nu}_\mu$.

Neutrino flavor analyses of contained atmospheric neutrino events have been performed by six different proton decay experiments, three of the water Cherenkov type and three iron calorimeters. Owing to a significant cancellation in systematic uncertainties, the experimental results are expressed in terms of the following

double ratio

$$R = \frac{(N_\mu/N_e)_{DATA}}{(N_\mu/N_e)_{MC}},$$

with N_x being the number of events identified as x-like in either the data or the MC event sample. The inverse R^{-1} is obtained if N_e/N_μ is used in this ratio.

The NUSEX[49] experiment took data from 1982 through 1988, shielded by 5000 MWE in the Mt. Blanc tunnel between France and Italy. The detector was a tracking calorimeter of 134 1-cm thick horizontal iron plates interleaved with planes of plastic streamer tubes. The streamer tubes had a cross section of $9 \times 9\,\mathrm{mm}^2$. The detector was cubic, its sides 3.5 m long. Of a total mass of 150 t, 130 t were assigned to the fiducial volume. It had no dE/dx capability, but its ability to unambiguously determine the flavor of incident neutrinos had been tested in particle and neutrino beams at CERN. Thirty-two muon-like events and 18 electron-like events were observed with lepton energies above 200 MeV. This was deemed in good agreement with a MC prediction of 36.8 and 20.5 events respectively, leading to an R^{-1} of $0.96^{+0.32}_{-0.28}$ from an exposure of 0.7 kty.

The Frejus[50] detector was operated between 1985 and 1988 in another highway tunnel connecting France and Italy (between Modane and Bardonecchia under the Alps), where the overburden corresponds to 4850 MWE. Nine hundred twelve iron plates of 3 mm thickness were stacked horizontally and interleaved with layers of Geiger and flash tubes in a parallelepiped of $6 \times 6 \times 12.3\,\mathrm{m}^3$. Hits in the $15 \times 15\,\mathrm{mm}^2$ Geiger tubes provided the trigger for the $5 \times 5\,\mathrm{mm}^2$ flash tubes. For every eight layers of flash tubes, there was one layer of Geiger tubes. While no dE/dx measurement was possible with this detector, its fine granularity allowed a stochastic energy loss measurement. A 700 t fiducial volume, out of a total 900 t detector mass, was used in the atmospheric neutrino analysis. Of 158 fully and 58 partially contained events collected in an exposure of 2.0 kty, 75 were identified as electron-like, 125 as muon-like, and 16 as NC neutrino interactions. MC predictions for these classes are given as 81.4, 136.2, and 14.5 respectively, resulting in $R = 1.00 \pm 0.15(stat.) \pm 0.08(syst.)$.

The total sample of neutrino-induced events in the Frejus experiment includes upward-going stopping and horizontal through-going muons as well. Since this detector could not resolve the direction of a track, the upward-stopping muon sample of 48 events is expected to contain 11 events that are really downward-going atmospheric muons. The angular acceptance for horizontally through-going

muons was chosen to limit the possible contamination by atmospheric muons to one event, leaving 44 events in this sample. Including these events in the analysis, the ratio becomes $R = 0.99 \pm 0.13(stat.) \pm 0.08(syst.)$.

Frejus and NUSEX use all their contained event data in the atmospheric neutrino analysis, including multitrack events from CC interactions and NC events. Their analysis was motivated by Kamiokande's observed anomaly in the flavor composition of its events, and its subsequent confirmation from the IMB water Cherenkov data (see below). Within their limited statistics, these two iron calorimeter experiments do not observe such an anomaly, which long resulted in the curious situation that iron calorimeters measured $R = 1$, while water Cherenkov detectors obtained $R = 0.6$. Inevitably, this raised the question of the respective technology's ability to distinguish electron showers from muon tracks. While the iron calorimeters' ability to identify showers by their lateral spread, which contrasts sharply to the single trail of hits observed along a muon track, rightfully went undisputed, the water Cherenkov community's claim to easily pick out the blurred rings projected by electron showers from the muons' sharp-edged ones drew criticism. This was finally settled by an experiment at the Japanese national accelerator center KEK, where electron, muon, and pion beams were injected into a 1 kt "model" of the Kamiokande detector.[51] Water Cherenkov detectors have no problem separating electron- from muon-like events.

The Soudan-2 experiment[52] was the first to break ranks with the other iron calorimeters. Located in a mine in Soudan, Minnesota, USA, it is shielded by an overburden of 2100 MWE. Data-taking began in 1989, with a quarter of the final detector size. Construction was completed at the end of 1993. The Soudan-2 detector consists of 244 modules totalling 963 t detector mass. A module occupies an area of $1 \times 1.3\,\mathrm{m}^2$, stacking 241 layers of precision corrugated steel sheets with 7560 drift tubes sandwiched between them. A module is 2.7 m high. In the tubes, ionization charge is drifted from the center outwards for detection in one of the two proportional chamber planes mounted on the module sides, enclosing the drift tubes. The proportional chambers allow two-dimensional readout over an area of $1 \times 2.7\,\mathrm{m}^2$ each. The detector hall is lined with a double layer of proportional tubes to actively veto outside radiation. Like the water Cherenkov detectors, but unlike the other iron calorimeters, Soudan-2 excludes events with more than one charged track. Using all events not vetoed by shield hits yields 80 "track" type events and 119 "shower" type events from a 2.83 kty exposure. Expecting 87.9 muon-like

events and 84.5 electron-like events from MC, the double ratio becomes $R = 0.65 \pm 0.09$. The remaining background, such as γ-rays or neutrons entering the detector, can be subtracted statistically, yielding $R = 0.61 \pm 0.14(stat.)^{+0.05}_{-0.07}(syst.)$. The detector is expected to accumulate a total exposure of 5 kty by 1999.

While suffering in resolution, the big advantage of water Cherenkov detectors is their huge mass, easily read out with PMTs on their inner surface. The high threshold for protons (1.4 GeV) helps suppress NC background, as recoiling nucleons rarely exceed this threshold. A charged particle above the Cherenkov threshold will emit light into a forward Cherenkov cone. For water Cherenkov counters, single track events will be referred to as single-ring events. Track direction and orientation are unambiguously projected onto the PMTs by the Cherenkov cone, and vertex reconstruction from relative timing information reaches a precision better than 1 m throughout the vast volumes.

The IMB[53] experiment was located in the Morton Salt Mine in Cleveland, Ohio, USA. Its $18 \times 17 \times 22.5\,\mathrm{m}^3$ water tank was shielded by an overburden of 1570 MWE and read out by 2048 eight-inch PMTs.[§] Installation in a salt mine meant low background from radioactivity, which does not affect the physics analysis at these energies, but still is relevant for detector performance. To enhance light collection, waveshifter plates were mounted on all PMTs. Out of its 6.9 kt total mass, 3.3 kt were used as fiducial volume. Data were taken with the IMB-3 detector through the years 1986 to 1991, when the detector was destroyed by rupture of its liner. Contained events were selected in the momentum ranges 100–1500 MeV for electrons and 300–1500 MeV for muons, both lower thresholds corresponding to the same visible energy in the detector of 100 MeV. From a total exposure of 7.7 kty, 610 single-ring events were extracted, 378 of which were found electron-like and 232 muon-like, the corresponding MC expectations yielding 291.7 and 320.7 events respectively. From the numbers quoted in the paper, the double ratio can be computed as $0.54 \pm 0.05(stat.) \pm 0.11(syst.)$. No zenith angle or momentum dependence is seen in the data.

Kamiokande[¶] gave an updated result[54,55] on contained events within energy ranges of 100–1330 MeV for electrons and 200–1500 MeV for muons, from a total exposure of 7.7 kty, as $R = 0.60^{+0.06}_{-0.05}(stat.) \pm 0.07(syst.)$. It is based on the observation of 248 electron-like and 234 muon-like single-ring events, a sample

[§]Now being used in the Super-Kamiokande anticounter.

[¶]See the solar neutrino section for a description of the experiment.

referred to as the sub-GeV data. The fiducial volume for this analysis contains 1.35 kt of the 4.5 kt total mass.

In a subsequent Kamiokande paper,[55] fully- and partially-contained events with visible energies > 1.33 GeV were analyzed. A hundred ninety-five fully-contained events were recovered from a 8.2 kty exposure, and 35 of them were discarded as multi-ring. This left 21 electron-like events and 73 muon-like events in this so-called multi-GeV sample. The fiducial volume for partially-contained events is reduced to 1.04 kt. Multi-ring events were allowed into the partially-contained event sample, while electron-like events were explicitly excluded. This left 104 partially-contained muons from a 6 kty exposure. Combining these two samples yields a double ratio $R = 0.57^{+0.08}_{-0.07}(stat.) \pm 0.07(syst.)$. One of the suggestions[56] proposed to solve the atmospheric neutrino problem was proton decays in the earth, leading to an excess in ν_e from a channel $p \to e^+\nu\nu$. Such a mechanism should clearly not contribute to the multi-GeV sample, where the mean neutrino energies are 5 GeV for the electron-like and 7 GeV for the muon-like events, and it can therefore be ruled out.

While the angular correlation between the outgoing lepton and the incoming neutrino is relatively poor for the sub-GeV data (RMS $\sim 60°$), it becomes fairly good for the multi-GeV data (RMS 15–20°). Since the distance between the production point and detector (the baseline for a neutrino oscillation experiment) varies with the zenith angle, for both the sub-GeV data and the multi-GeV data, the double ratio was plotted over the cosine of the zenith angle. No structure is seen in the sub-GeV data, but a striking zenith-angle distribution emerged for the multi-GeV data, prompting a first oscillation analysis of atmospheric neutrino data, which yielded allowed regions in the ($\sin^2 2\Theta$, Δm^2) parameter spaces for both $\nu_\mu \to \nu_e$ and $\nu_\mu \to \nu_\tau$ oscillation. While the corresponding parameter space for $\nu_\mu \to \nu_e$ oscillation conflicts with exclusion regions obtained in reactor experiments, $\nu_\mu \to \nu_\tau$ oscillation with maximal mixing and $\Delta m^2 \sim 10^{-2}$ eV^2 still remains a valid explanation of the atmospheric neutrino anomaly. Disappearance of ν_μ into sterile neutrino species can also accommodate the data.

The Kamiokande result on atmospheric neutrinos is also confirmed by the Super-Kamiokande[‖] experiment. Its large statistics now supersede the original Kamiokande results. As for the solar neutrinos, two independent analyses were

[‖]See also the solar neutrino section for a general description of the detector.

initially performed on the Super-Kamiokande data, giving increased confidence in the combined result as well as the original Kamiokande measurement. Having provided the desired cross-check for one another, these two analyses have now been merged to optimize the overall performance of the Super-Kamiokande analysis tools. Specific results and the corresponding plots from the Super-Kamiokande analysis can be seen in Y. Itow's lecture in these proceedings. This 50 kt water Cherenkov detector with its 22.5 kt fiducial volume already statistically dominates all atmospheric neutrino measurements, with 25.5 kty exposure for fully-contained events and 22.8 kty exposure for partially-contained events, after a little more than one year's operation. Due to the much larger detector size, events are contained up to much higher energies than in previous detectors, yet for comparison the numbers for electron- and muon-like events given below are extracted using the Kamiokande cuts for the sub-GeV data (which were motivated not by detector dimensions, but by the initial focus of the experiment and its trigger and analysis on proton decay, setting a scale of $\sim 1\,\mathrm{GeV}$).

A neutrino oscillation analysis of the complete Super-Kamiokande atmospheric neutrino sample under the assumption $\nu_\mu \to \nu_\tau$ yields an allowed region significantly shifted towards lower Δm^2 with respect to the corresponding Kamiokande analysis. A small overlap remains around $\Delta m^2 \simeq 5 \times 10^{-3}\mathrm{eV}^2$, with the Super-Kamiokande region extending all the way down below $\Delta m^2 = 10^{-3}\mathrm{eV}^2$ at maximal mixing.

In the ICARUS experiment (see the solar neutrino section for details), atmospheric neutrino reactions will be detected above the energy threshold for the CC reaction on argon nuclei.[57] The threshold is 25 MeV for ν_e and 130 MeV for ν_μ reactions. Partial neutrino/antineutrino discrimination can be achieved even without a magnetic field, through identification of the recoil proton in the lepton final states. For the recoiling neutrons associated with antineutrino interactions, some nuclear activity is expected in the volume surrounding the interaction. For a sensitive mass of 540 t in a 600 t module, 80 muon-like and 60 electron-like events are expected from CC interactions per year (under the assumption of no oscillation) for a combined fully and partially contained event sample.

3.2.2 Upward-Going Muons

Upward-going muons allow no energy determination. Moreover, data on upward-going muons sample a target mass under the detector, that throughout the muon range depends on the neutrino energy. Only muon type neutrinos are detected this way.

Given the uncertainties in absolute flux calculations, no conclusion can be drawn from the absolute rates of observed events, which follow the general trend of the low-energy data for muon-like events and are lower than theoretical predictions. Zenith-angle distributions can be extracted with the baseline ranging now from 5×10^2 km to 1.3×10^4 km for events originating in a hemisphere under the detector.

Collection of this kind of data is no longer an exclusive privilege of large proton decay detectors. Large area multilayered horizontal scintillator arrays have measured upward-going muons. Yet their acceptance tends to vanish near the horizontal direction, making significant geometric corrections necessary. Two experiments using layers of liquid scintillator for time-of-flight discrimination between upward- and downward-going muons reported their latest results at the TAUP97.** The Baksan Underground Telescope[58] consists of four layers of $17 \times 17\,\mathrm{m}^2$ and the MACRO[59] detector contains three such layers of $12 \times 77\,\mathrm{m}^2$ surface each.

Detectors providing the necessary granularity allow the ratio of upward stopping to upward through-going muons to be used to obtain information on the energy spectrum of the observed muons. IMB used that technique to obtain an exclusion plot for oscillation parameters largely overlapping with the Kamiokande allowed region.[60] This result was subsequently criticized because of the cross sections used in the analysis,[61] yielding a substantially-reduced excluded region on the basis of an improved cross-section estimation. While this new excluded region no longer overlaps with the old Kamiokande allowed region, it now is in conflict with the oscillation parameters derived in the Super-Kamiokande contained event analysis. An analysis of the ratio of upward stopping to through-going muons for the Super-Kamiokande detector is underway.

Altogether no definite conclusions concerning neutrino oscillations have as yet been drawn from the analysis of data on upward-going muons.

**Proceedings or preprints were not yet available at the time of writing. See also the summary talk on atmospheric neutrinos by E. Kearns at this workshop.

4 Conclusion

Solar neutrinos pose a serious problem when confronted with our best knowledge of astrophysics and elementary particle physics. Our current understanding of all phenomenology involved seems to leave little to no room to accommodate the observational data through manipulations of the solar models (in spite of the obvious simplifications they are based on), while a relatively unsurprising extension of the well-tested minimal Standard Model of particle physics (i.e., nonzero neutrino mass) does exactly that. A new generation of experiments, well-designed to provide some of the missing pieces in this puzzle, is just becoming operational. At the same time, a set of new and still more ambitious experimental techniques is being developed for future application to this specific problem.

The atmospheric neutrino anomaly is emphasized again by the high statistics data just becoming available from new experiments, and neutrino oscillation still is the only scenario explaining the experimentally observed signatures. Although the downward shift in Δm^2 implied by the Super-Kamiokande data will make things more difficult for the planned accelerator-based long-baseline neutrino oscillation experiments, in the current situation it will ultimately be their job to either confirm or refute this interpretation.

It is an exciting time in the deep mines and tunnels around the world.

Acknowledgments

Apart from the many helpful discussions I had with and comments I got from my colleagues at ICRR and the Kamioka Observatory, I would especially like to thank Dave Casper of UC Irvine for his careful reading of my messy draft. If there still is fault in my writing, it probably occurred where I did not heed his advice.

Many thanks to Michael Altmann of TU Munich for providing the GALLEX and Borexino figures, and to Jaret Heise of UBC Vancouver for the SNO figure. K. Lande of U. Penn. Philadelphia and V. N. Garvin of INR Moscow helped with valuable input to my Chlorine Experiment and SAGE figures.

But I need to issue a **warning**: With the exception of the one of Super-Kamiokande, the figures that I drew up myself cannot ultimately be trusted. They reflect my best knowledge and understanding at the time of writing this report. The reader can identify them by the little hollow head and stomach figure throwing up its arms (1.8 m or 5 ft. 11 in. from head to toe).

References

[1] J. N. Bahcall, these proceedings.

[2] S. Wojcicki, these proceedings.

[3] J. N. Bahcall and R. Davis, Science **191**, 264 (1976).

[4] K. S. Hirata *et al.*, Phys. Rev. Lett. **63**, 16 (1989).

[5] A. I. Abazov *et al.*, Phys. Rev. Lett. **67**, 332 (1991).

[6] A. Anselmann *et al.*, Phys. Lett. B **285**, 376 (1992).

[7] J. N. Bahcall and M. H. Pinsonneault, Rev. Mod. Phys. **67**, 781 (1995).

[8] S. Degl'Innocenti *et al.*, Astroparticle Phys. **7**, 77 (1997).

[9] J. N. Bahcall *et al.*, *Solar Neutrinos—The First Thirty Years* (Addison-Wesley, 1994), pp. 97-106.

[10] J. N. Bahcall, Rev. Mod. Phys. **50**, 881 (1978).

[11] B. T. Cleveland, Nucl. Instrum. Methods **214**, 451 (1983).

[12] M. B. Aufderheide *et al.*, Phys. Rev. C **49**, 678 (1994).

[13] R. Davis, D. S. Harmer, and K. C. Hoffman, Phys. Rev. Lett. **20**, 1205 (1968).

[14] K. Lande and P. S. Wildenhain, in *Proceedings of the International Conference on Neutrino Physics and Astrophysics NEUTRINO '96*, edited by K. Enqvist *et al.* (World Scientific, 1997), p. 25.

[15] R. Davis, Nucl. Phys. B **48**, 284 (1996).

[16] A. Kopylov, in *Proceedings of the International Symposium on Neutrino Astrophysics, Takayama, October 1992*, edited by Y. Suzuki and K. Nakamura (Universal Academy Press, 1993), p. 157.

[17] J. N. Bahcall, Phys. Rev. C, **56**, 3391 (1997).

[18] P. Anselmann *et al.*, Phys. Lett. B **342**, 440 (1995).

[19] P. Anselmann *et al.*, Nucl. Instrum. Methods A **378**, 233 (1996).

[20] W. C. Haxton, Phys. Rev. C **38**, 2474 (1988).

[21] J. Engel, S. Pittel, and P. Vogel, Phys. Rev. C **50**, 1702 (1994).

[22] Y. Fukuda *et al.*, Phys. Rev. Lett. **77**, 1683 (1996).

[23] J. N. Bahcall and M. Pinsonneault, Rev. Mod. Phys. **64**, 885 (1992).

[24] D. R. O. Morrison, in *Proceedings of the International Conference on High-Energy Physics (ICHEP'94)* Glasgow, Scotland, July 1994, 983 (1995).

[25] F. Reines, Proc. Roy. Soc. A **301**, 159 (1967).

[26] R. S. Raghavan, S. Pakvasa, and B. A. Brown, Phys. Rev. Lett. **57**, 1801 (1986).

[27] G. Bellini, Nucl. Phys. B **48**, 363 (1996).

[28] J. N. Bahcall *et al.*, Phys. Lett. B **178**, 324 (1986).

[29] P. Benetti *et al.*, Nucl. Instrum. Methods A **332**, 395 (1993).

[30] P. Cennini *et al.*, Nucl. Instrum. Methods A **345**, 230 (1994).

[31] P. Cennini *et al.*, Nucl. Instrum. Methods A **355**, 660 (1995).

[32] R. Dolfini *et al.*, Preprint INFN/AE-97/49.

[33] T. Ypsilantis *et al.*, Preprint CERN-LLA/95-11.

[34] A. Pallares *et al.*, Nucl. Instrum. Methods A **367**, 181 (1995).

[35] T. Ypsilantis *et al.*, Preprint CERN-LLA/96-05.

[36] S. R. Bandler *et al.*, Phys. Rev. Lett. **68**, 2429 (1992).

[37] S. R. Bandler *et al.*, Phys. Rev. Lett. **74**, 3169 (1995).

[38] R. S. Raghavan, Phys. Rev. Lett. **37**, 259 (1976).

[39] R. S. Raghavan, Phys. Rev. Lett. **78**, 3618 (1997).

[40] M. Honda *et al.*, Phys. Rev. D **52**, 4985 (1995).

[41] T. K. Gaisser *et al.*, Phys. Rev. D **53**, 1314 (1996).

[42] T. K. Gaisser *et al.*, Phys. Rev. D **54**, 5578 (1996).

[43] T. Stanev, Nucl. Phys. B **48**, 165 (1996).

[44] G. L. Fogli and E. Lisi, Phys. Rev. D **52**, 2775 (1995).

[45] T. Kajita, *Physics and Astrophysics of Neutrinos*, edited by M. Fukugita and A. Suzuki (Springer, 1994).

[46] T. J. Haines *et al.*, Phys. Rev. Lett. **57**, 1986 (1986).

[47] K. S. Hirata *et al.*, Phys. Lett. B **205**, 416 (1988).

[48] L. V. Volkova, Sov. J. Nucl. Phys. **31**, 784 (1980).

[49] M. Aglietta *et al.*, Europhys. Lett. **8**, 611 (1989).

[50] K. Daum *et al.*, Z. Phys. C **66**, 417 (1995).

[51] S. Kasuga *et al.*, Phys. Lett. B **374**, 238 (1996).

[52] H. Callagher at WIN97; W. W. M. Allison *et al.*, Phys. Lett. B **391**, 491 (1997).

[53] R. Becker-Szendy *et al.*, Phys. Rev. D **46**, 3720 (1992).

[54] K. S. Hirata *et al.*, Phys. Lett. B **280**, 146 (1992).

[55] Y. Fukuda *et al.*, Phys. Lett. B **335**, 237 (1994).

[56] W. A. Mann, T. Kafka, and W. Leeson, Phys. Lett. B **291**, 200 (1992).

[57] F. Cavanna, Nucl. Phys. B **35**, 280 (1994).

[58] M. M. Boliev, in *Proceedings of the International Cosmic Ray Conference*, Rome, Italy, 686 (1995).

[59] S. Ahlen *et al.*, Phys. Lett. B **357** 481 (1995).

[60] R. Becker-Szendy *et al.*, Phys. Rev. Lett. **69**, 1010 (1992).

[61] P. Lipari, M. Lusignoli, and F. Sartogo, Phys. Rev. Lett. **74**, 4384 (1995).